UNIVERSITY OF CALIFORNIA

SANTA CRUZ

MODELING AND DESIGN OF LOW IMPEDANCE MICROELECTRODES FOR BIOMEDICAL APPLICATIONS

A dissertation submitted in partial satisfaction
of the requirements for the degree of

DOCTOR OF PHILOSOPHY

in

ELECTRICAL ENGINEERING

by

Shirin Zarrabi

March 2013

The Dissertation of Shirin Zarrabi
is approved:

_____
Professor Michael Isaacson, Chair

_____
Professor Joel Kubby

_____
Professor Showei Chen

_____
Tyrus Miller
Vice Provost and Dean of Graduate Studies

Contents

List of Figures:

Dedication and Acknowledgement

This work is dedicated to the memory of my father who always encouraged me through my educations. It is also dedicated to my mother who was always there for me, to my sister who was always kind and helpful, to my husband for supporting me and to my daughters for helping me every step of the way with their patience and joyful smiles.

It is with immense gratitude that I acknowledge the support and help of my advisor Dr. Michael Isaacson. I am grateful for his patience, motivation, enthusiasm, and knowledge. His guidance and keen insights have been invaluable to my research.

I am very thankful to Dr. Holger Schmidt and specially Dr. Tom Yuzvinsky for helping with Focused ion beam machine.

I'm also grateful for the advice, recommendations, and support of Dr. Joel Kubby, Dr. Shaowei Chen, and Dr. Ali Shakouri throughout my graduate studies.

I would like to thank my friends in our group who have helped me throughout these years by their support.

MODELING AND DESIGN OF LOW IMPEDANCE MICROELECTRODES FOR BIOMEDICAL APPLICATIONS

by

Shirin Zarrabi

Abstract

Microelectrodes are devices through which neural signals are obtained or delivered. The goals for designing microelectrodes are maximum selectivity (ability to select and record from a single cell) and minimum impedance. It is very important to reduce the impedance of metal microelectrodes as much as possible since the main source of noise for metal microelectrodes is thermal noise which is directly related to impedance. Signal to noise ratios are particularly important in the quality of the signal that can be received by the microelectrode.

In order to increase selectivity, small size microelectrodes are desired but as the size of the microelectrode decreases the impedance increases so fabrication of small size microelectrodes with low impedance is always a challenge.

To reduce the resistance of microelectrodes a traditional approach is electroplating them with platinum black, however the impedance of the microelectrode, using this method, is generally unstable. Creating microstructures on electrodes is another approach that has been tried before without a significant success.

This work investigates the problems with the design of microstructures and introduces a novel design and technique to fabricate microelectrodes with significantly lower impedance than traditional flat microelectrodes, yet more stability than the platinum black coating approach.

Introduction

The widespread use of microelectronic techniques, together with the extensive utilization of in vitro cultures, is making it more and more feasible to obtain an intimate junction between cultured neurons and flat microelectronic transducers. It is one of the principal tools of neurophysiologists interested in the nerve system at the cellular level.

An electrode is a device which transduces bioelectric signals to and from electronic signals. Despite the prevalence of such devices there remains a good deal of mystery about how best to make these electrodes and how to interpret the extracellular potential that they record.

Biomedical microelectrodes should be **biocompatible** (nonreversible reaction between the microelectrode and the solution is not desired), moreover corrosion of the microelectrode is not acceptable because these reactions would be either toxic to the cell or they would change the normal environment and function of the cell.

Several materials have been used for biomedical electrodes .Noble metals such as **platinum** and **iridium** are the most common [1] but other materials such as **Iridium oxide**, **Titanium nitride**, **Tantalum pentaoxide and Carbon (fibers or nanotubes)** have also been used [2]-[4]. **Gold** can be used for recording [1].

Because extracellular signals are weak, it is important to have low noise microelectrodes.

Since the main source of noise is thermal noise, it is important for the microelectrodes to have low impedance.

Neural probes are usually metallic probes, but there have been some experiments using

MOSFETs to record signals from neurons acting as their gates [5]. However, the noise generated by field-effect transistors is higher than metal electrodes [6].Therefore in this thesis we have concentrated on microelectrodes.

The goals for designing microelectrodes are:

1- Maximum selectivity (which means smaller size so we can select a single neuron for recording- The range of neuron sizes is 4- 100μm)
2- Minimum impedance for maximizing signal to noise ratio.
3- Stability

As the size of the microelectrode decreases the impedance increases, so fabrication of small size microelectrodes with low impedance is always a challenge.

To reduce the resistance of microelectrodes, a traditional approach is electroplating them with platinum black which makes pores on the surface of the metal so the effective surface will increase because of roughness (without increasing the apparent area) and resistance will decrease. However the impedance of the microelectrode, using this method, because of weak adherence to the underlying metal, is generally unstable [7].

Creating microstructures with platinum on electrodes is another approach that has been tried before, but the reduction of impedance more than 5 times compared to a flat microelectrode has not yet been achieved (see chapter 1).

This paper will investigate the problems associated with the design of microstructures and will introduce a novel design and technique to fabricate microelectrodes with significantly lower impedance than traditional flat microelectrodes, yet more stability than the platinum black coating approach.

Chapter 1
Microelectrode Modeling

Electrode Modeling

Different equivalent circuits have been proposed before for a metallic probe in saline Electrolyte [7], [8]. Two of these equivalent circuits will be described in this paper.

Here are a few facts about neural probing that will be used later:

- Bio-electric potentials are carried in electrolytic media in the form of ionic currents.
- The mobility of ions is approximately six orders of magnitude lower than that of electrons and holes.
- Bioelectric signals usually will not have frequencies more than 10 kHz.

Capacitance

When a metallic object is placed in an ionic solution there will be a space charge build up at the interface. This space charge layer represents a capacitance [7].

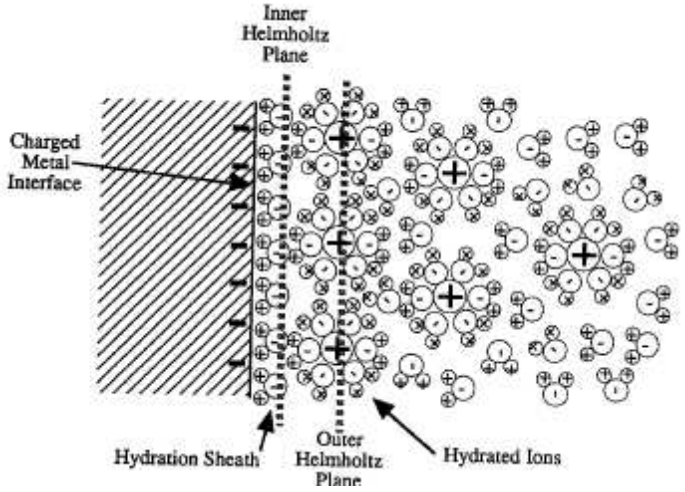

Fig. 1. Double layer and Helmholtz planes [7]

If we put a metal electrode in a water solution, water molecules will be oriented according to the electrode charge and will form a hydration sheath in contact with surface of metal. (Hydrogen is positive and Oxygen in negative).After this hydration sheath there will be hydrated ions which are the ions in solution with opposite charge of the metal and surrounded with oriented water molecules. These two layers (double layer) will form two parallel planes (known as Helmholtz planes) and act as a capacitor.[7]

$$C_H = \varepsilon_0 \varepsilon_r \, A/d \qquad (C_H \text{ for Helmholtz plane})$$

ε_0 is the dielectric permittivity of free space ($\varepsilon_0 \approx 8.854\times10^{-12}$ F m^{-1});

ε_r is the relative permittivity (sometimes called the dielectric constant) and for water its value is 78.54 at 25 C° but can be as low as 6 in the interface so

$$\frac{C_H}{A} = 5.3\cdot10^{-11} \,/\, d \qquad \text{(Capacitance per unit area)}$$

Assuming d=5A° , C_H will be 0.11 F/m²

Charge diffuses from electrode to the solution as anions and cations. This diffusing charge also results in another capacitance which can be derived by applying Gauss's law to the charge near the electrode [9].

$$C_D = \frac{\varepsilon_0 \varepsilon_r}{L_D} \cdot \cosh\left(z\, V_0 / 2V_t\right)$$

Where z is the charge of ions (we can assume z=1 for saline solutions), V_t=kT/q=26mv (V_t is known as thermal voltage at room temperature, k is the

Boltzmann constant, T is tempreature and q is the magnitude of the electrical charge on the electron with a value of 1.602×10^{-19}) and V_0 is the potential at the electrode.

L_D is Debye length and is given by [7]:

$$L_D = \sqrt{\frac{\varepsilon_0 \cdot \varepsilon_r \cdot V_t}{2n_0 \cdot z^2 \cdot q}}$$

n_0 is the bulk number concentration of the ion in question(moles/liter=0.154 for saline, times Avogadro's number 6.02205 x 10^{23} #/mole). This value for physiological saline at 25° is $0.154 \times 6.02205 \times 10^{23} = 9.3 \times 10^{22}$ ions/liter or 9.3×10^{25} ions/m³

These two capacitors in series will make the total interface capacitor (C_I)

$$1/ C_I = 1/ C_H + 1/ C_D$$

As the concentration of solution or the applied voltage is increased, the space charge region will be more compact and the magnitude of C_D will increase while C_H remains the same. So by increasing the voltage, the capacitance will increase until C_H dominates (0.11 F/m). Figure 2 shows C_I for different ε_r from top to bottom ε_r values are 78.54,50 and 6 respectively [7].

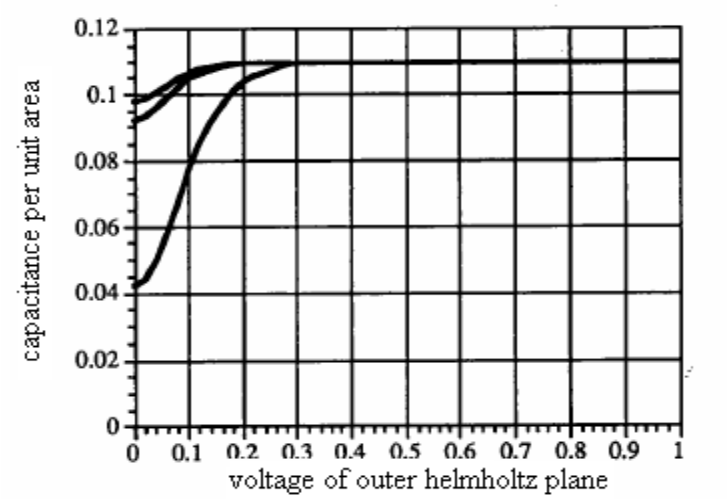

Fig. 2. C_I for different ε_r

Resistance

There are 3 important components in the resistive model of an electrode.

1-Charge transfer to space charge in solution (through the electrode)

2-Diffusion of ions to and from the electrode

3- Chemical reactions at the electrode

Charge transfer

The charge transfer current density between the electrode and solution is given by the Butler-Volmer Equation [10]

$$J = J_0[e^{[(1-\beta).z.(V-V_0)/V_t]} - e^{(-\beta.z.(V-V_0)/V_t)}] \quad \text{in A/cm}^2$$

Where J_0 is the exchange current density, V_0 is electrode voltage without current flow and V is electrode voltage with current flow, z is the charge of the ion and β is a symmetry factor which is the difference in energy barriers to electronation and deelectronation and hence the symmetry of positive and negative charge flow.

Electronation and deelectronation are the transfer of electrons between the oxidized and reduced form of reactant. Values of J_0 are given in the table below.

Table I
Exchange current density for noble metals [7]

Material/Reaction	**J_0(A/cm²)**
Gold in buffered saline	2×10^{-9}
Oxygen reaction	4.5×10^{-6}
Au, hydrogen reaction	3.98×10^{-6}
Pt, hydrogen reaction	7.94×10^{-4}
Ir, hydrogen reaction	200×10^{-4}

If β is 0.5 then we have

$$J = 2J_0 \sinh[z(V - V_0)/2V_t]$$

and charge transfer resistance can be calculated as:

$$R_t = \partial V / \partial J \quad \text{in } \Omega.\text{cm}^2$$

Using this definition and the area of the microelectrode the total resistance can be calculated.

Now V-V0 for **neural recording** is small so $\sinh[z(V - V_0)/2V_t] \approx z(V - V_0)/2V_t$

=> $$R_t = V_t / AJ_0 z \quad \text{in } \Omega.\text{cm}^2$$

And V-V0 is high for **neural stimulation** so

$$\sinh[z(V - V_0)/2V_t] \approx \frac{e^{z(V - V_0)/2V_t}}{2}$$

=> $$R_t = \frac{2V_t}{J_0 . A} e^{-z(V-V_0)/2V_t}$$ in Ω.cm²

Diffusion

a- DC condition

For any electrode there is a limiting or saturation current due to the fact that the current will be carried to the solution by diffusion of ions. This steady state diffusion is related to the electrode current density by [7]:

$$J / J_s = 1 - e^{-|V-V_0|z/V_t}$$

So

$$R_d = \partial V / \partial J = V_t / z[1/(J_s - J)] \qquad \Omega.cm^2$$

This equation is good for currents near DC (steady state diffusion).

b- AC condition

The impedance for a sinusoidal voltage due to diffusion in electrolyte is given by [11], [12]:

$$| Z_d | = k / \sqrt{f}$$

Where f is the frequency of the sinusoidal voltage.

This is based on the assumption that applying a sinusoidal voltage will force a sinusoidal spatial concentration of ions, so by increasing the frequency, the concentration gradient will increase at the electrode interface and more electrode current will be possible.

This impedance can be modeled as a resistor and capacitor (series or parallel).

For the parallel equivalent (W indices are given since this has been proposed by Warburg [11], [12])

$$Z_w = (1/R_w + j2\pi.f.C_w)^{-1}$$

Where R_w and C_w can be calculated as $R_w = 1/2\pi.f.C_w$ and $R_w = 10^6 \frac{V_t}{z^2 q n^0 A\sqrt{\pi f D}}$. D is the diffusion coefficient in cm²/sec and A is the area of electrode in cm².

For saline, the Warburg impedance is small compare to R_t in the range of 100 Hz to10 KHz and often will not be included in the model because the time scale is so short that diffusion cannot manifest itself.

Considering: $V_t = 26mv$

$q = 1.6\times10^{-19}$

$n_0 = 9.3\times10^{25}$ (as calculated before)

$z = 1$ (for saline)

$$\left(R_w = 10^6 \frac{26\times10^{-3}}{1.6\times10^{-19}\cdot 9.3\times10^{25}.A\sqrt{\pi.f.D}} = \frac{9.86\times10^{-5}}{A\sqrt{D}} \; for 100Hz \right)$$

Chemical reaction

This is only present when a slow chemical process becomes the rate-limiting factor in the overall reaction at the electrode (for example an ion required for an intermediate electrochemical reaction in short supply due to a slower reaction that produces it).

Then the current leaves the electrode to the solution. The solution can be modeled as a resistor by integrating the resistance of solution shells outward from electrode.

$$R_s = \int_0^{\infty} dR_s$$

R_s is the resistance of the solution.

For a planar disk electrode with one side exposed .One can show analytically that R_s is given by [13]:

$$R_s = \rho / 4r$$

Where ρ is conductivity of solution in Ω.cm (72 Ω.cm for saline).

By direct analogy to thermodynamic shape factors used in heat flow problems, the equation for a planar rectangular electrode will be [14]:

$$R_s = \frac{\rho \ln(4l / w)}{\pi l}$$

Where *l* and *w* are the length and width of rectangle in cm. The equation for a square electrode can be calculated when $l = w = a$.

The equivalent circuit for the electrode for this model is seen in Figure 3.

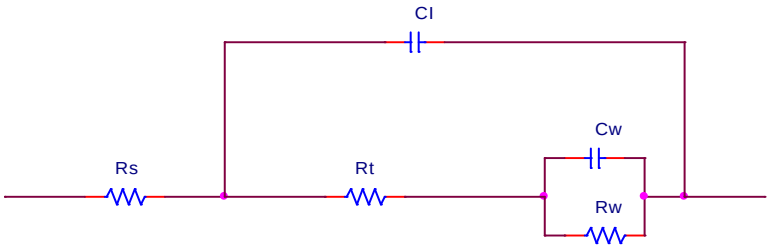

Fig. 3. Equivalent circuit of electrode

By making nonplanar microelectrodes and also surface roughening, the impedance can be reduced because there will be more area for current. Modeling of porous surfaces is difficult. In general they can be modeled as transmission lines but since we cannot accurately measure or predict pore sizes, the impedance is given with a scaling factor (K) that is fitted to experimental data [15].

$$Z_p = (1 - j)K / \sqrt{f}$$

So the equivalent circuit with porous surface considerations will be Fig.4.

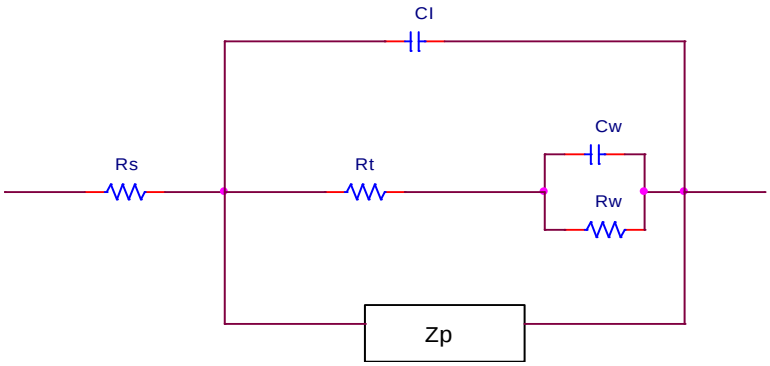

Fig. 4. Equivalent circuit of a porous electrode

Platinizing, which increases the effective surface area by a spongy deposit of platinum black, will reduce these impedances by two orders of magnitude [7].

There are also parasitic elements in every circuit. These parasitic elements are listed below:

a) Resistance of interconnects

$$R_c = \rho L / A$$

for most metals ρ is in order of $10^{-5}\,\Omega.cm$

b) Capacitance of interconnects to the electrolyte through a passivation layer

$$C_p = \varepsilon_0 \varepsilon_r LW / d$$

or an improved approximation which takes into account sidewall contributions [16].

$$C_p = 1.15\varepsilon_0\varepsilon_r LW/d + 2.80\varepsilon_0\varepsilon_r L(t/d)^{0.222}$$

c) Capacitance between the interconnects and substrate through silicon dioxide (or other passivation layer) C_s

d) Coupling capacitance between interconnects [16].

$$C_c = 2\varepsilon_0\varepsilon_r L[0.03(W/d) + 0.83(t/d) - 0.07(t/d)^{0.222}](s/d)^{-1.34}$$

which takes into account only two nearest neighbor conductors and *s* is the spacing between them.

Fig. 5 shows the parasitic impedances.

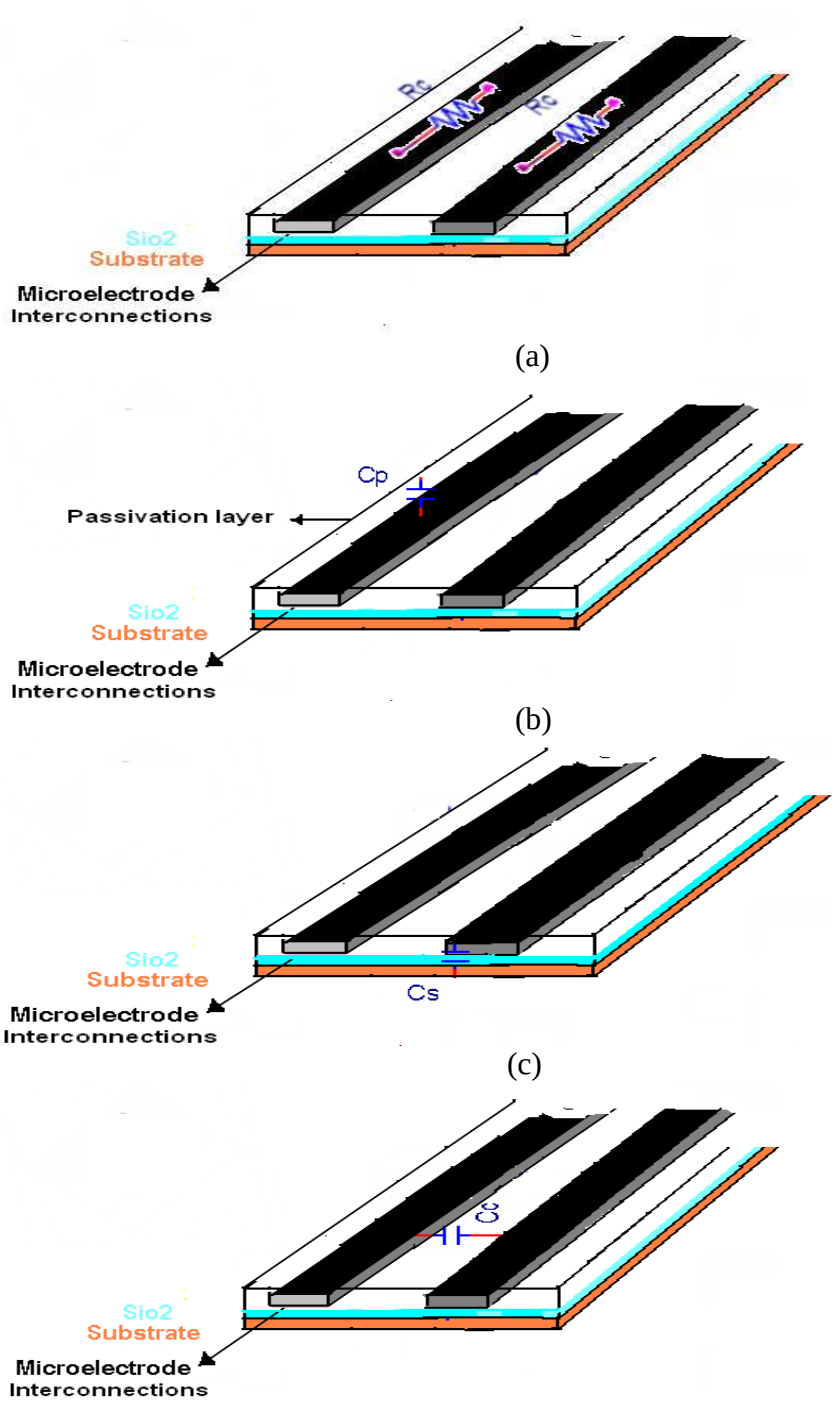

Fig. 5. Parasitic elements of electrode

(a) Resistance of interconnects

(b) Capacitance of interconnects to the electrolyte through passivation layer

(c) Capacitance between the interconnects and substrate

(d) Coupling capacitance between interconnects

With all these considerations, the whole model will look like Figure 6.

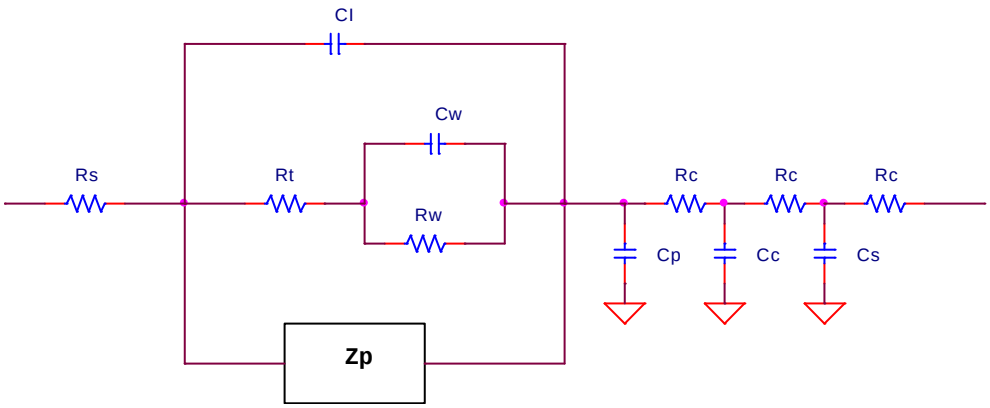

Fig. 6. Equivalent circuit of electrode with all considerations taken into account

A Different Modeling Approach

Fig. 7. shows another approach to modeling the microelectrodes [8].

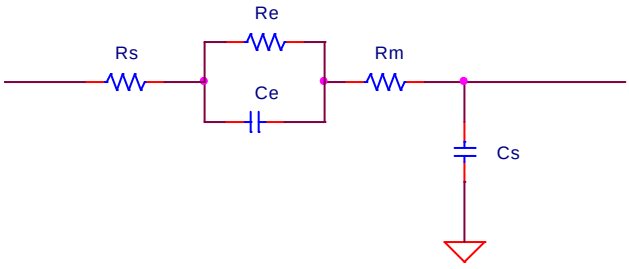

Fig. 7. Equivalent circuit of electrode (different approach)

Here Cs is the capacitance of all parasitic elements. This includes the capacitance from the metal of the electrode to the bath through the insulation as well as the accumulated capacitance of all the connectors and (shielded) wires. The formula for the capacitance across an insulating material of relative dielectric constant ε_r

between a center conductor (the electrode metal) of diameter d and a concentric outer conductor (the electrolyte bath) of diameter D is given in as [8]:

$$C_s = \frac{0.245 \cdot \varepsilon_r}{\log_{10}(\frac{D}{d})} \text{ pF/cm}$$

Rm is the parasitic resistance of the metallic portion of microelectrode.

Ce is the capacitance of the electric double layer at the interface of the metal tip and the electrolyte solution.

The electric double layer constitutes quite literally an electrolytic capacitor. Its value for bright platinum at 1 kHz is about 20μF/cm² or 0.2pF/μ². There are different reports on measuring this value [8]. By platinizing, capacitance Ce will increase from 0.2 pF/μ² to 60 pF/μ² (a ratio of 300 to 1). It does not, however, behave as a simple lumped capacitor of constant value. If one plots the real and imaginary parts of the electrode impedance over the frequency range of 100 Hz to 10 kHz, both Ce and Re appear to vary with frequency [17].

The rate at which these parameters decrease with increasing frequency depends upon the presence of compounds adsorbable onto the metal, the diffusion rate of the ionic reactants such as oxygen in the vicinity of the tip, the rate constants of the reactions themselves, and the presence of polarizing currents from external direct-current sources.

The most common testing solution for metal microelectrodes is physiological saline,

and there it is found empirically that both Re and Ce vary as $1/\sqrt{\omega}$ (ω is angular frequency- $\omega = 2\pi f$, ω has been used here instead of f to keep formulas with the same format in reference 8) while the phase angle, which is equal to $\tan^{-1} \omega Ce\,\mathrm{Re}$, remains close to 45° (Fricke's law [19]). This behavior indicates that the simple parallel resistor and capacitor is an inadequate model of the process. Since the liquid plate of the capacitor is a charge distribution in a conducting medium in which diffusion must play a role, the impedance would seem to be more adequately described by a distributed rather than a lumped parameter network. Indeed, a transmission line with a high series resistance and large shunt capacitance per unit length is one such distributed model. Its input impedance varies as $1/\sqrt{\omega}$.

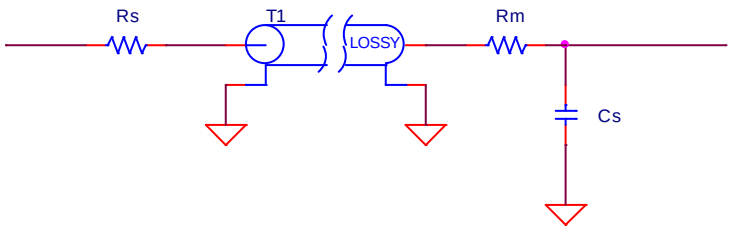

Fig. 8. Equivalent circuit of electrode using transmission line model

In practice, the recording of extracellular spike activity is done over the bandwidth of 100 Hz to 10 kHz, and the impedance measured at the commonly accepted mean frequency of 1 kHz is quite adequate to specify tip properties. So Ce can be calculated using 20 μF/cm² or 0.2 pF/μ² and then using $\tan^{-1} \omega Ce\,\mathrm{Re}$ =1, Re can be calculated. It is also possible to model with series resistance and capacitance but as ω approaches zero in the real case, the condition $\omega Ce\,\mathrm{Re}$ = 1 breaks down, and at dc, since the tip

resistance is finite, the parallel circuit is more appropriate than the series. Over the frequency range of interest here, the series and parallel circuits may be considered interchangeable. Re is the leakage resistance due to charge carriers crossing the electric double layer. Using classical kinetic theory from the rates at which an ion will pass over an energy barrier at temperature T by thermal agitation [8]:

$$i = i_0 e^{F\Delta V / 2RT} - i_0 e^{-F\Delta V / 2RT}$$

F is the Faraday constant (F = 96,485.3365 C/mol), R is the gas constant and T is temperature.

For voltage changes of less than a few millivolts this expression may be replaced by the linearized equation.

$$i = i_0 \frac{F}{RT} \Delta V \quad \text{A/cm}^2$$

Since RT/F is about 26 mV at room temperature, the resistance of the electrode may be expressed as $R_e = \frac{\Delta V}{i} = \frac{26mv}{i_0}$

i_0 is the same as j_0 in the previous model but this will be a DC model and Re will change with frequency and will be calculated using Ce.

Rs is the resistance of the saline bath between the metallic interface and infinity (the indifferent or ground electrode). This is sometimes called the spreading resistance (The same Rs we had in previous model).

The spreading resistance of the saline bath is easily found. Imagine a spherical tip of radius r. The resistance of a thin spherical shell of saline at radius r of thickness dr of specific resistivity ρ is

$$dR_s = \rho \frac{dr}{4\pi.r^2}$$

Integrating from re to infinity yields

$$R_s = \int_r^{\infty} dR_s = \frac{\rho}{4\pi.r}$$

Using 72.5 Ω.cm for ρ, one can find that for a 1-μ tip R_s, is 115 kΩ, for a 2-μ tip, it is 57 kΩ, and for a 5-μ tip, 23 kΩ. For tips of other than spherical shapes the above formula is not exact, but clearly this resistance is generally negligible when compared to Z_e. For example, the 2-μ tip can have an unplantinized impedance of 89 MΩ. Platinizing will lower this to 1.0 MΩ against which the value of 0.057 MΩ is small enough to be neglected. Thus, regardless of tip shape, R_s is much less than Z_e (this is certainly true of unplatinized tips) and consequently can be neglected.

New Considerations

Let's look at part of our first model (Figure 6) and discuss the accuracy of this part of the model (see Figure 9).

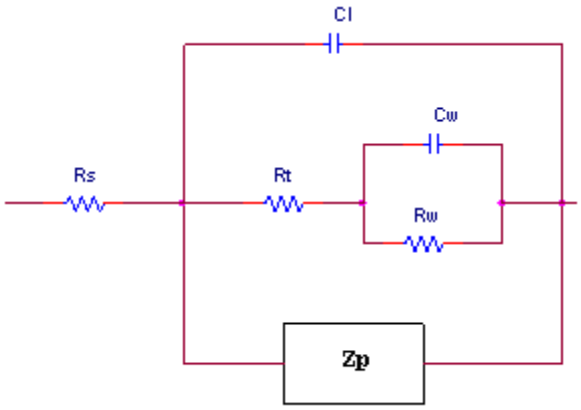

Fig. 9. Part of first model (in Figure 6)

For interface capacitance, although ideal capacitive behavior has been observed with liquid mercury electrode systems (which have perfectly smooth surfaces), there are many situations, especially with solid metal electrodes, where the high-frequency impedance characteristic is not as expected .The two most likely causes of the observed frequency dependence of Z_I (Interface impedance) are specific adsorption and surface roughness effects[18]. With solid biomedical electrodes, the major source of the observed frequency dispersion (β<1) is probably due to the surface roughness of the electrodes. That is why we have Z_P in our model. It has been observed that the impedance locus of the interface impedance, Z_I , is well represented by a straight line at an angle Φ to the real axis and given by the empirical equation[18]:

$$Z_I = K(j\omega)^{-\beta}$$

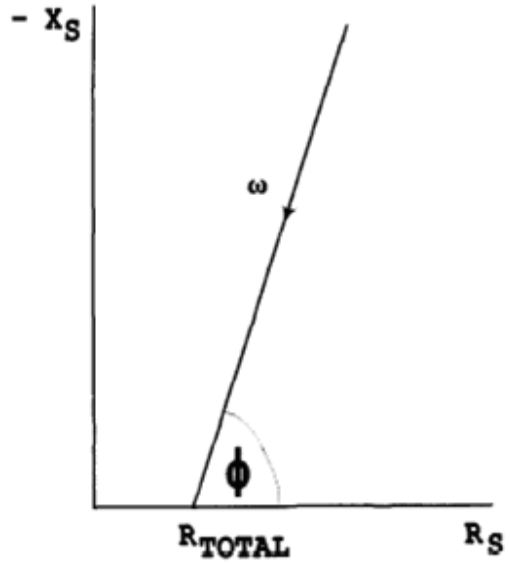

Fig. 10. Interface impedance of electrode

X_S is the imaginary and R_S is the real part of Z_I.

where K is a measure of the magnitude of Z_I, β is a constant which has a value between 0 and 1, (typically 0.8 for many biomedical electrode systems). R_{total} is actually $R_{spread}+R_{electrod}$ It has been observed (Fricke, 1932) [19] that the phase angle, Φ, is related to the fractional power, β, such that

$\Phi = \beta\pi / 2 \quad (90\beta$ degrees)

This empirical relationship represents the impedance of the double layer capacitance in the presence of surface roughness effects. β is related to the degree of surface roughness; the rougher the surface, the lower the value of β. K also decreases with surface roughness. As the phase angle of the impedance is constant, the interface impedance has been termed a “constant phase angle” (CPA) impedance.

Some researchers have wrongly equated the constant phase angle impedance to the diffusion, or 'Warburg' impedance which has a constant phase angle of 45 ° (i.e. $\beta = 0.5$), however, β is generally larger than 0.5[18].It is usually close to, although less than, unity.

Many attempts have been made to interpret the effect that surface topography has on the form and magnitude of the interface impedance. The best known model [20] is that the impedance, Zo, of pores on the electrode surface could be represented by transmission lines. This model successfully explains qualitatively many aspects of interface impedance. The many assumptions and approximations made, however, limit its ability to represent accurately measured impedance data. This model can only interpret constant phase angle behavior where $\beta = 0.5$ and it is therefore not optimal.

More complex transmission line models have since been suggested [21, 22, 23]. Although these models have been found to reproduce measured impedances more accurately, many of them include arbitrary and questionable assumptions and the increased number of variables involved makes the drawing of meaningful conclusions difficult. At present microelectrodes are usually tested and the measured data fitted to the empirical equation [24].

There has been also interest in Mandelbrot's work [25] on fractal geometry to model electrode impedance. According to the fractal concept, a single parameter, the fractal dimension, D, is capable of characterizing a rough surface without the need of a detailed description (McAdams, 1990)[26].The idea is based on an empirical formula proposed by Richardson[27]. According to Richardson, if you measure the length of

an irregular line by following its shape with a small interval of length ε you will need $F\varepsilon^{-D}$ intervals of length ε to cover the whole line due to the fact that when ε gets smaller you will need more intervals .

The length of the line then will be the number of intervals multiplied by the length of interval $L(\varepsilon) = F\varepsilon^{1-D}$. D is a measure of the irregularities of line.

Mandelbrot proposed that D should be interpreted as dimension so a straight line will have a dimension of D=1 and any other irregular line will have a dimension of more than one but less than 2 and the same way an irregular surface will have a dimension more than 2 but less than 3.This theory has been used to find a relationship between D (fractal dimension) and β the fractional power of the CPA element by calculating the surface of a rough material and considering capacitance of the surface.

The effective dimension can directly be measured by light and X-ray scattering [28, 29] and by optical or electron microscopic image analysis [30].

Several attempts have been made to derive an equation relating the fractal dimension of a surface to the interface impedance. Such fractal models can be broadly classified into three categories: hierarchical, fractal branching of single pores (Liu, 1985) [22]; fractal distributions of surface pore diameters (Sapoval, 1987) [31]; fractal scaling of the interface (Nyikos & Pajkossy, 1985) [32]. The first two kinds of models involve the use of transmission lines/ladder networks.

Using fractal scaling concepts, Nyikos & Pajkossy (1985) [32] have derived the following expression for the interface impedance, Z_I, in the presence of surface effects:

$$Z_I = R_{total} + A[Z_s]^{\beta}$$

where Z_s is the anticipated interface impedance in the absence of surface effects, β is a fractional power (0.5<β<1) related to the fractal dimension of the electrode surface, A is a proportionality constant which contains all frequency-independent factors (such as a geometric descriptor) and R_{total} is the sum of the series resistances due to the leads and the electrolyte ($R_{spread} + R_{electrode}$).Nyikos & Pajkossy [32] proposed that

$$\beta = \frac{1}{D-1}$$

At high frequencies, the interface impedance Z_s, is dominated by that of the double-layer capacitance, C_I. So

$$Z_I = R_{total} + K(j\omega)^{-\beta} \quad \text{where } K = A(C_I)^{-\beta}$$

At low frequencies, the interface impedance is quite well represented by an equivalent circuit model incorporating, in parallel, a resistance and a constant phase angle impedance (Z_{CPA}), this impedance is equated with the double-layer capacitance distorted by surface roughness effects and the parallel resistance with that due to charge transfer.

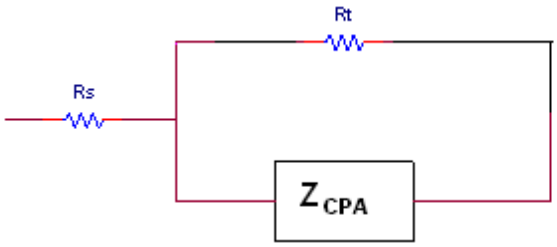

Fig. 11. Equivalent circuit of electrode

The impedance is given by

$$Z_I = \frac{R_t}{1 + (j\omega)^{\beta}.R_t / K}$$

It is naive, however, to think that surface effects will only distort capacitance and will have no effect on R_t, as assumed in the above model. It is more realistic that surface effects will affect the parallel combination of both. However, the above equation is a useful approximation which allows qualitative interpretation of experimental results.

Conditions that affect the model

The electrode-electrolyte interface impedance becomes non-linear, i.e. deviates by more than 10% from its linear small-signal value, at a certain limit voltage, V_L, which is independent of the frequency of the applied signal. $V_L = \frac{40}{n}$ mv, where n is the number of electrons per molecule oxidized or reduced [18].

There is also a limit current of linearity i_L, with this empirical relationship for many electrode systems over wide frequency ranges [18]:

$$i_L = B\omega^{\beta}$$

where B is a constant particular to the electrode system and β is the fractional power .The presence of a parameter describing the frequency dependence of the linear interface impedance in a relationship describing the non-linearity of the system is intriguing. Unfortunately, no satisfactory physical explanation has been given in the literature.

The constant phase angle impedance is relatively linear over a wide range of applied potentials. The charge transfer resistance, R_t on the other hand, derived from the Butler-Volmer equation, is very non-linear, even for small signal amplitudes. It has therefore been suggested that R_t is the major source of observed non-linearities.

As low frequencies' impedance is dominated by R_t, the effects of such non-linearity will be first evidenced at these frequencies [18].

Coatings of electrodes, open circuit potential (which is the potential naturally occurring between working and reference electrode) and time are also reported to change the parameters of model [33].

FET-Based Sensors

It has been mentioned before that one can use FETs to record signals from neurons acting on their gates. An electrolyte replaces the metal gate in an *electrolyte oxide silicon field effect transistor* (*EOSFET*). Local voltage recording by an *EOSFET* has to be distinguished from the application of an *EOSFET* as an *ionsensitive transistor* (*ISFET*). For ISFETs molecular interactions of protons and

other ions in the electrical double layer modulate the threshold voltage. Here we are dealing with a genuine modulation of the gate voltage [6].

ISFETS

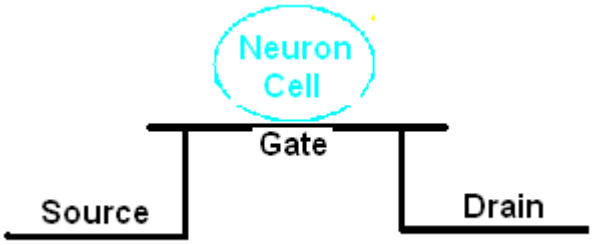

Fig. 12. Using FET to record from neurons

The ion sensitive field effect transistor (ISFET), invented in 1970 by Bergveld [34], is a solid-state device that combines the chemically sensitive membrane with the MOS type field effect transistor. In its extensive study over the past 35 years, ISFET has been characterized and measured, indicating drawbacks related to: thermal-dependency, long term drift and hysteresis. These factors limit the accuracy of ISFET-based measurements systems, especially for biomedical and analytical applications.

Changes in the pH of the electrolyte produce variations on the threshold voltage due to ionic activity at the electrolyte–insulator interface. Hence, the measurement of the threshold voltage of the ISFET directly changes with the pH concentration of the electrolyte. The device operation of an ISFET can be deduced from both the pH-dependent characteristic of threshold voltage and the MOSFET behavior. In fact, the

ISFET devices are commonly biased in the triode region (i.e. $V_{DS} \leq V_{GS} - V_T$), where the drain current I_{DS} is expressed as follows:

$$I_{DS} = K[(V_{GS} - V_T^*) - \frac{V_{DS}}{2}] \cdot V_{DS}$$

where K is the device transconductance factor, V_{DS} is a drain-source voltage and $V_T^* = V_T + EPH$ denotes the ISFET's threshold voltage resulting from the threshold voltage (V_T) of FET and EPH is the interface potential between sensing membrane and buffer solution [35].

The drift in ISFETs is the shift of $\frac{\partial V_{GS}}{\partial t}$ under constant current I_{DS}. According to the principles of ISFETs, the shift of $\frac{\partial V_{GS}}{\partial t}$ is the same as $\frac{\partial V_T}{\partial t}$, and one can get the drift of ISFET by the measurement of $\frac{\partial V_T}{\partial t}$. The drift is independent of the electrolyte. When t <

1000 h, the amount of the drift is approximately constant. And if t > 5000 h, it is close to zero [36].

The response of an ISFET to a fast pH step is in general characterized by a fast response, followed by a slow change in the same direction, and ultimately a drift which is linear or logarithmic with time T [37].

Time response data show that the intrinsic response time is of the order of a few milliseconds or faster. The presence of a slow response occurs with a delay of the order of minutes to hours after the pH variation [36].

The phenomenon called drift is a slow, continuous, change of the threshold voltage of an ISFET in the same direction. It is difficult to identify the cause of this phenomenon, which could be either a surface or a bulk effect, or both. Polarization effects or ion migration in the gate insulator may cause a slow drift of the sensor signal at the temperatures normally used [38], [36].

Calculating SNR of Microelectrodes and FET Based Sensors

Extracellular signals are usually less than 1mV, so noise and signal to noise ratios (SNR) are particularly important in the quality of the signal that can be received by the sensor.

In this section we are going to calculate the SNR of a microelectrode array based on "Extracellular Recordings From Patterned Neural Networks Using Planar Microelectrode Arrays" IEEE Transaction on Biomedical Engineering, Vol. 51, No 9, September 2004 [24] and compare it with FET based sensors reported in "Silicon Chip for Electronic Communication between Nerve Cells by Non-invasive Interfacing and Analog-Digital Processing" Advanced Materials 2002, 14, No.17, September 3 [5].

The microelectrode's impedance has been modeled with this formula $Z_e = R_0 f^m$ ($f = \frac{\omega}{2\pi}$, f has been used here to be consistent with the paper) and the impedance has been measured over the range of 100 to 5000 Hz and was fit to the model using linear regression. For gold they measured $R_0 = 1.4 \times 10^8$ and m=-0.69 and for a platinized microelectrode they have $R_0 = 1.1 \times 10^5$ and m=-0.36 and also they have reported an estimation of R_{spread} of 58k and 19k for gold and platinized microelectrodes respectively.

Now the noise for a resistive element can be calculated as [39]:

$$V_n = \sqrt{4KT \int_{f1}^{f2} (Z_e + R_{spread}) df}$$

where K is the Boltzman constant and T is temperature.

So for gold $V_n = \sqrt{4 \times 1.38 \times 10^{-23} \times 300 \int_{100}^{5000} (1.4 \times 10^8 f^{-0.69} + 58000) df} = 8.85 \mu V$

And for platinum $V_n = \sqrt{4 \times 1.38 \times 10^{-23} \times 300 \int_{100}^{5000} (1.1 \times 10^5 f^{-0.36} + 19000) df} = 1.46 \mu V$

For FET Based sensors it is assumed that one can use MOSFET formulas for calculations.

In reference [5] it has been reported that:

"The bulk of the interfacing chip was kept at +6.5V with respect to the bath held on ground potential with a Ag/AgCl electrode and the source at +3-3.5V.The drain was

connected to a subdrain voltage of +2.5-3.5V through a resistance of 10.8KΩ.The total source-drain current at the working point was I_{SD} = 300-400μA.A change of voltage on gate of +10mV induced a current modulation of -1μA, as checked before each measurement"

Based on this information we conclude that the FET has been setup in the linear region. Now "A change of voltage on gate of +10mV induced a current modulation of -1μA" So $g_m = \frac{1\mu A}{10mV} = 100\times10^{-6}$ Since we have 10.8k at drain, this current modulation should create 10.8mV modulation in output voltage so we have a gain of $\frac{10.8}{10} = 1.08$ we know $gain = g_m \cdot r_o$ so $r_o = \frac{1.08}{100\times10^{-6}} = 10.8k$

To calculate the thermal noise in the FET we use this formula:

$$V_n^2 = 4kT\frac{2}{3}g_m r_o^2 = 4\cdot1.38\times10^{-23}\cdot300\cdot\frac{2}{3}\cdot100\times10^{-6}\cdot(10800)^2 = 1.29\times10^{-16} \quad V^2/Hz$$

[39]

Also we have flicker noise in a FET which can be calculated as [40]:

$V_n^2 = \frac{Kg_m^2 r_o^2}{C_{ox}WL}\cdot\frac{1}{f}$ where K is a process dependent constant of the order of 10^{-25}

In this paper also it has been reported that length and width of gate were 2μm and 8μm and the oxide layer was 10nm.

So

$$C_{ox} = \frac{\varepsilon_0\varepsilon_r}{t_{ox}} = \frac{8.85\times10^{-12}\times3.9}{10\times10^{-9}} = 3.45\times10^{-3} \quad (F/m^2)$$

$$V_n^2 = \frac{10^{-25}.(100\times10^{-6}\cdot10800)^2}{3.45\times10^{-3}.2\times10^{-6}.8\times10^{-6}}\cdot\frac{1}{f} = 2.11\times10^{-12}\frac{1}{f} \quad (V^2)$$

And finally the 10.8k resistor which is used to bias the transistor is a source of thermal noise like any other resistance.

$V_n^2 = 4kTR = 4 \cdot 1.38 \times 10^{-23} \cdot 300 \cdot 10800 = 1.78848 \times 10^{-16}$ So the total noise will be:

$$V_n = \sqrt{\int_{100}^{5000} 1.78848 \times 10^{-16} + 1.29 \times 10^{-16} + 2.11 \times 10^{-12} \frac{1}{f} df} = 3.12 \mu V$$

To summarize the noise calculations:

Table II
Comparison of gain and noise

	FET Sensor	***Microelectrode(platinum)***	***Microelectrode(gold)***
gain	1.08	1	1
noise	3.12μV	1.46μV	8.85μV

For FET sensor Pmos is usually used since they are less noisy [41]. g_m and r_o will determine the noise. r_o has power of 2 so to have less noise r_o should be as low as possible but gain ($g_m \cdot r_0$) should be kept more than 1 because after that the output signal will be weaker than original one. The best setup may be to increase g_m as much as possible and then to reduce r_o until the gain is around one.

In the linear region $g_m = 2kV_{DS}$ so V_{DS} can be increased up to $V_{GS} - V_T$ if linearity of response is desired.

In 1968 Piet Bergveld has modeled in-phase interference voltage on source and drain of FET sensors with the equivalent circuit shown in Figure 13. These interferences occur because long wires will bridge the distance between sensor and amplifiers and measuring devices so the interferences can be coupled to them through interface

capacitances and FET capacitances (especially when there are multiple sensing points there would be crosstalk on these wires.). He discussed that to cancel the influence of interference voltages, FET should be biased far below saturation region and resistance on drain and source should be equal ($R_d = R_s$) [34].

Also since it is known that V_T of these sensors is constantly changing it is better to bias these sensors in the linear region so changes of V_T will have less influence on recording voltages.

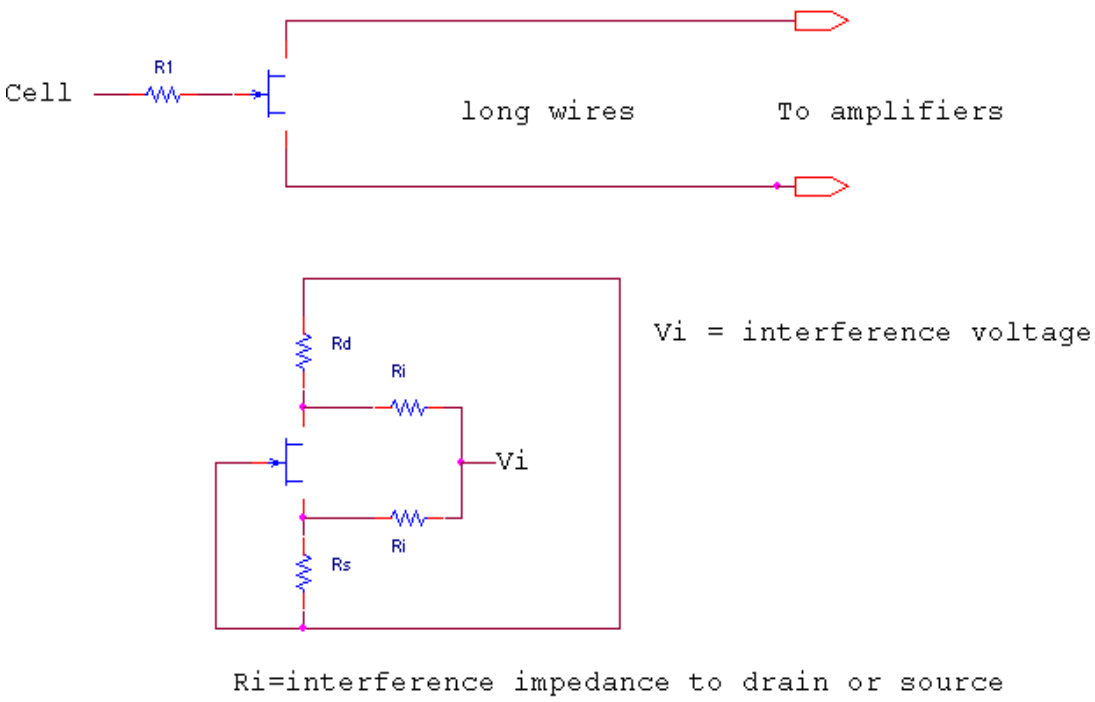

Fig. 13. Equivalent circuits of FET sensors

In summary the noise generated by field-effect transistors is substantially higher than in metal electrodes because of both thermal noise and $\frac{1}{f}$ noise and also drift as

discussed. In metals, platinum has the lowest impedance and thus the lowest thermal noise.

For platinized microelectrode, noise will come mostly from R_{spread} which is electrolyte impedance but for gold noise will come mostly from interaction between microelectrode and electrolyte (Z_e).

Methods of Reducing Impedance in Metal Microelectrodes

It is very important to reduce the impedance of metal microelectrodes as much as possible since the main source of noise for metal microelectrodes is thermal noise which is directly related to impedance.

To reduce the impedance, several methods have been used in the past.

1- A traditional approach to reduce the microelectrode impedance is electroplating them by platinum black which makes pores on the surface of metal so the effective surface will increase and resistance will decrease.

The impedance of the microelectrode, because of the weak adherence of platinum black to the underlying metal, will be unstable by deposition of platinum black alone because it can easily break. Marresse [42] discussed electroplating under ultrasonic agitation so only those platinum particles that can endure the agitation, survive and become part of the electrode. Increases in surface area of such electrodes up to 18 times over non-plated and up to 6 times over non-ultrasonically plated platinum black electrodes has been reported.

Two orders of magnitude decrease in impedance are typically seen [7], [42].

While platinum black is a simple process that yields a large area increase, the approach is unreliable for long-term implantations because its flimsy dendritic structures are not mechanically robust and even a small dissolution rate would cause them to quickly lose their effectiveness.

2-Chemical modifications which are used to improve biocompatibility, cellular adhesion or controlling pattern of cultured cells on substrate will reduce the impedance by making a better connection between cells and microelectrode [7].

3-It is known that some platinides, in particular iridium will form highly conductive oxide layers in certain solutions under anodic conditions.

Microelectrodes coated with this oxidized, or activated, iridium exhibit considerably lower impedances than do those using unoxidized iridium (up to one order of magnitude). The main disadvantage of these electrodes is the uncertainty about how long the activated state persists under different conditions of use and storage.

The activated tip impedances are remarkably stable for periods of several hours of immersion testing and for brief periods of drying and rinsing in distilled water, However the microelectrodes occasionally appear to lose virtually all of their activation spontaneously after many hours of disuse in either the dry or wet states [43].

4-Creating microstructures with platinum on electrodes is another approach that has been tried several times before [44]-[48] but reduction of impedance more than 5 times compare to a flat microelectrode has not so far been achieved.

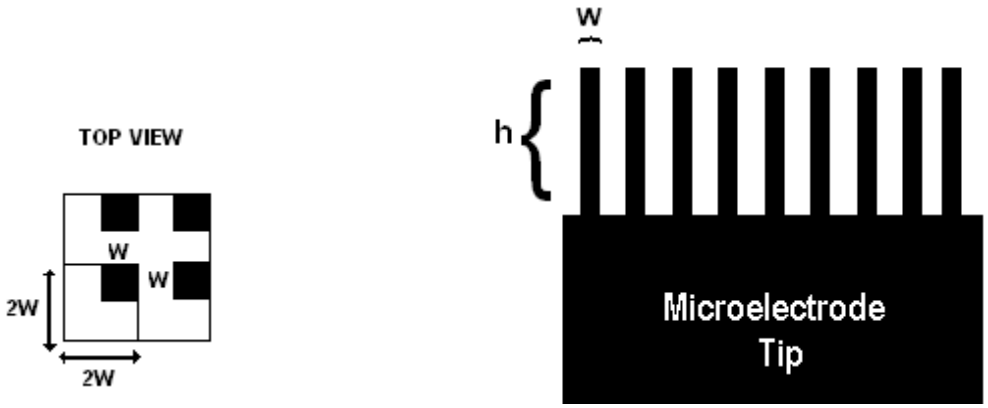

Fig. 14. Microstructures on microelectrode

In order to understand what we might expect from microstructured electrodes, a simple calculation for the reduction in impedance is given below.

If a flat electrode surface area $A_{flat} = (2w)^2$ is reshaped to include posts with a height h and width w, the total electrode surface area becomes $A_{post} = (2w)^2 + 4w.h$ .Thus in terms of post aspect ratio (h/w), the surface area is increased by a factor of $A_{post} = A_{flat}.(1 + h/w)$ .To make microstructures which are capable of reducing impedance comparable to platinum black deposition, $h/w = 107$ (maximum) [44].

To increase the density of the microstructures on the surface, a checkerboard arrangement can be used [45].

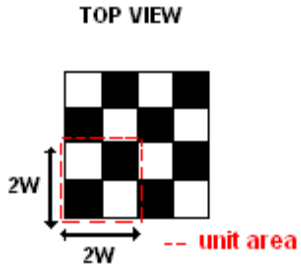

Fig. 15. Checkerboard arrangement of microstructures

In this case for the unit area:

$$A_{flat} = (2w)^2$$
$$A_{post} = (2w)^2 + 8w.h$$
$$A_{post} = A_{flat}.(1 + 2h/w)$$

If the microstructures are not in touch with each other and there is space between them then the area can be calculated as follow:

for the case of unit area=3w×3w

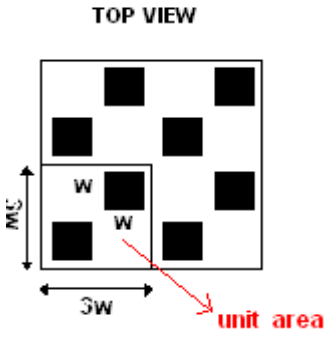

Fig. 16. Checkerboard arrangement of microstructures with space

$$A_{flat} = (3w)^2$$
$$A_{post} = (3w)^2 + 8w.h$$
$$A_{post} = A_{flat}.(1 + 8h/9w)$$

Or for any unit area with the size of αw × αw

$$A_{flat} = (\alpha.w)^2$$
$$A_{post} = (\alpha.w)^2 + 8w.h$$
$$A_{post} = A_{flat}.(1 + 8h/\alpha^2 w)$$

These formulas have been used in chapter 4 to calculate the expected results of the simulations. The numerical values for calculations have been given in Table III.

Table III

Numerical values for the calculations of A_{post}/A_{flat} with different parameters (all values are in μm)

	h	$\alpha = 2$	$\alpha = 2.5$	$\alpha = 3.25$	$\alpha = 4$	$\alpha = 5$
$w = 2$	10	11	7.4	4.78	3.5	2.6
	20	21	13.8	8.57	6	4.2
	30	31	20.2	12.36	8.5	5.8
	40	41	26.6	16.15	11	7.4

Thus, one expects that impedance reduction of more than one order of magnitude should be achievable and impedance reduction should be more than what has been shown in the literature. This will be discussed further in chapters 3-5.

Chapter 2
Neuron Modeling

The Biological Neuron

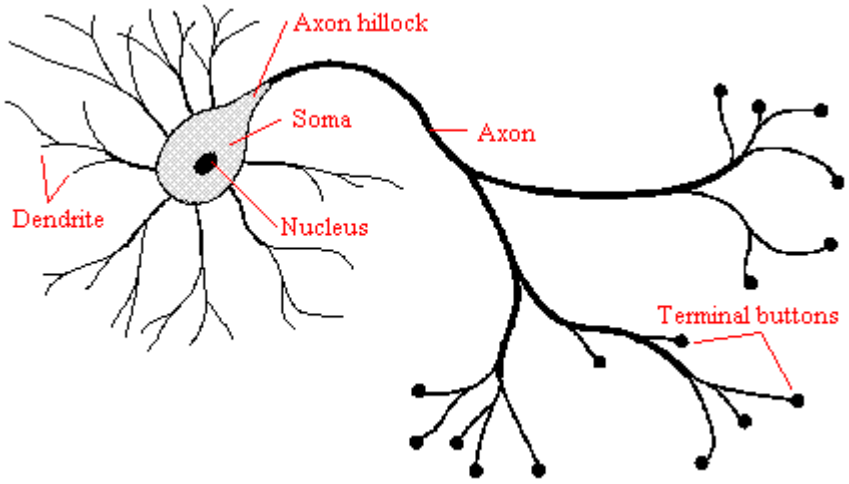

Fig. 17. Neuron [49]

Each neuron is a cell that uses biochemical reactions to receive, process and transmit information. A neuron's dendritic tree is connected to a thousand neighboring neurons. When one of those neurons fires, a positive or negative charge is received by one of the dendrites. The strengths of all the received charges are added together through the processes of spatial and temporal summation. Spatial summation occurs when several weak signals are converted into a single large one, while temporal summation converts a rapid series of weak pulses from one source into one large signal. The aggregate input is then passed to the soma (cell body). The soma and the

enclosed nucleus don't play a significant role in the processing of incoming and outgoing data. Their primary function is to perform the continuous maintenance required to keep the neuron functional. The part of the soma that does concern itself with the signal is the axon hillock. If the aggregate input is greater than the axon hillock's threshold value, then the neuron *fires*, and an output signal is transmitted down the axon. The strength of the output is constant, regardless of whether the input was just above the threshold, or a hundred times as great.

The output strength is unaffected by the many divisions in the axon; it reaches each terminal button with the same intensity it had at the axon hillock. This uniformity is critical in an analogue device such as a brain where small errors can snowball, and where error correction is more difficult than in a digital system.

Each terminal button is connected to other neurons across a small gap called a synapse. The physical and neurochemical characteristics of each synapse determine the strength and polarity of the new input signal. This is where the brain is the most flexible, and the most vulnerable. Changing the constitution of various neuro-transmitter chemicals can increase or decrease the amount of stimulation that the firing axon imparts on the neighboring dendrite. Altering the neurotransmitters can also change whether the stimulation is excitatory or inhibitory [50].

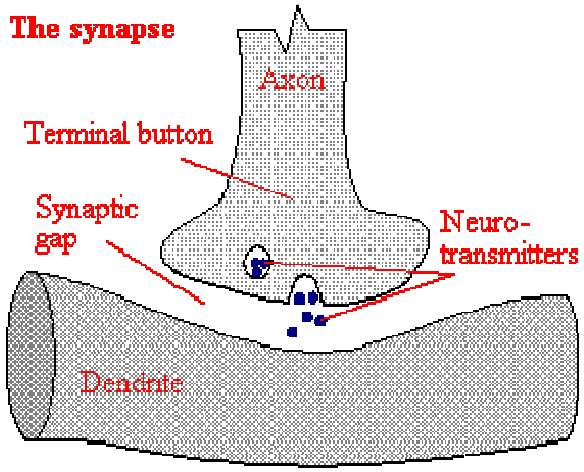

Fig. 18. Axon and dendrite at synapse (where two neurons connect)

Molecular Structure and Modeling

A cell membrane is composed of proteins (%60), lipids (%38) and carbohydrate (%1-2). There are 2 types of lipids, neutral lipids (cholesterol) and phospholipids. Phospholipids consist of 2 portions:

1- Nonpolar portion (2 long fatty acid chains)

2- Polar portion (contains charged phosphate groups)

In water or salt solution, lipids orient in a unique fashion. Polar groups are hydrophilic (water molecules are polar too) and fatty acids chains are hydrophobic so in water they will make a lipid bilayer.

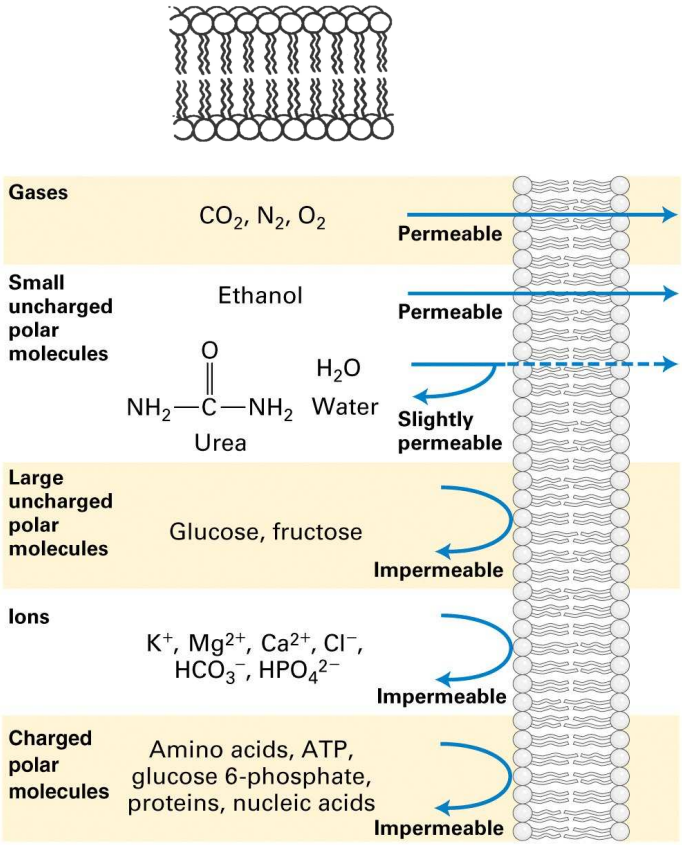

Fig. 19. Lipid bilayer [50]

The lipid bilayer is impermeable to ions, but the cells have ion pumps. Ion pumps are ion exchange mechanisms and ion transporters in the body of cell which keep a certain concentration of ions inside and outside the cell. This difference between ion concentrations inside and outside of the cell will make a voltage difference between inside and outside. (resting potential). Concentration differences are approximately [50]:

K^+ 100mM inside 5mM outside (20×)

Na^+ 10mM inside 150mM outside (15×)

Cl^- 5mM inside 110mM outside (22×)

Ca^{2+} 10^{-4} mM inside 5mM outside (50,000×)

These mechanisms are constantly working to keep the cell at resting potential. They are slow and are not responsible for information transmission.

Ion channels are protein lined pores in the cell body which can transport ions from one side to the other, their response is fast and they are responsible for information transmission. They usually have a mechanism which triggers the transportation of ions. The channels which do not have such mechanism contribute to a leakage current. Each channel will transport a special ion and those channels can be modeled by a voltage source and a resistance as shown below [51].

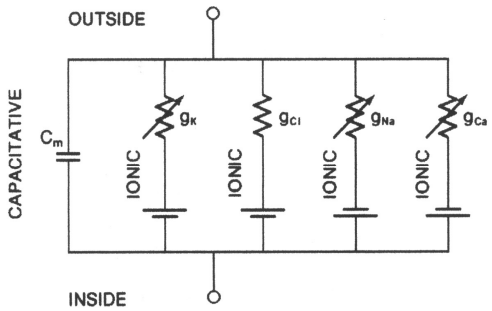

Fig. 20. Equivalent circuit of neuron cell

Modeling of the cells' activity of different neurons can be done using software such as "Neuron" from Duke and Yale Universities [52] or "Genesis" from Caltech [53]. Genesis works better on UNIX machines and Neuron can be run with windows.

These programs will calculate the intracellular potentials. Intracellular potential will pass to the outside of cell membrane through the ionic channels.

The membrane model shown above can be simplified as shown below. Using this model for cell membrane impedance, the intracellular signal can be converted to extracellular signal which will be received by a microelectrode.

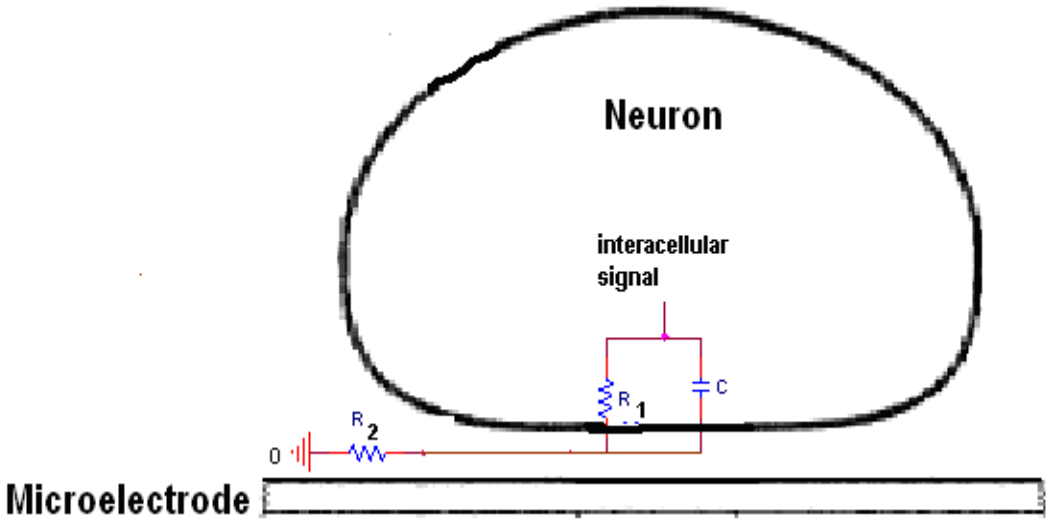

Fig. 21. Equivalent circuit of neuron in contact with microelectrode

C=membrane capacitance= $1(\mu f / cm^2) \times \pi a^2$

R1=membrane resistance= $0.1(ms / cm^2) \times \pi a^2$

a =cell's radius

R2=seal resistance= $\frac{\rho}{d \cdot 5\pi}$

ρ =specific resistance of electrolyte=72Ω.cm for saline

d =distance between cell and microelectrode=30nm [54]

R2 is the seal resistance. This resistance is there because the contact between the neuron cell and microelectrode is not perfect and there is always some current leakage to the electrolyte. The magnitude of this leakage, of course, depends on how good the neuron cell is sealed to the microelectrode. 30nm is an estimated seal distance between the cell and microelectrode [54].

Combining the cell model and the microelectrode model we can model the whole system as shown below. Note that to model a microelectrode, a simplified model called the Randles model has been used [55]. This model is basically the same as the first model that has been discussed except for parasitic impedances and Warburg impedances which are considered low in the range of frequencies of neuron activities.

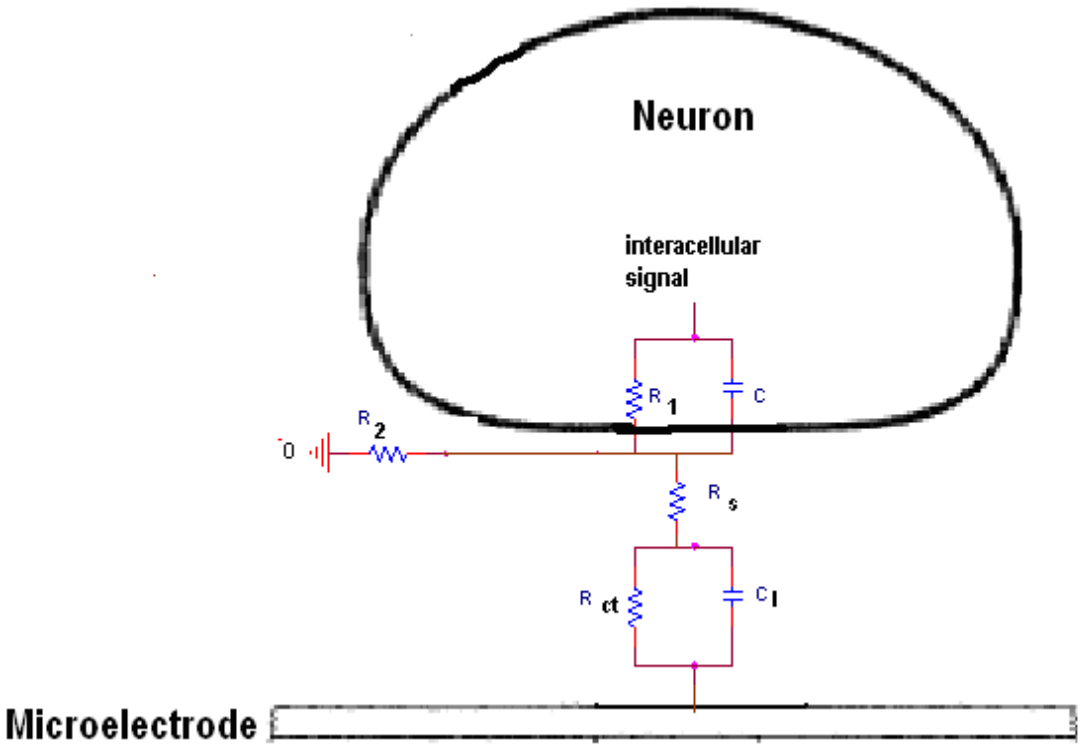

Fig. 22. Equivalent circuit of neuron and microelectrode

CI =Interface capacitance=CH+CD (double layer capacitance +diffusion capacitance)

Rct (R_t) = charge transfer resistance

Rs=solution resistance

Model Simulation

Using the neuron models described and “Neuron” software (to generate intracellular Potentials) and then entering the values into a circuit simulator (for example Spice [56]) and also an amplifier model, the output of the amplifier can be simulated and compared with actual recordings. The results should be close and the difference should be the result of model simplifications and noise.

Chapter 3
Wetting Calculations

There has been ongoing research on designing and fabricating of microstructures on microelectrodes in the past [44]-[48], but the reduction of impedance more than 5 times compare to a flat microelectrode has not been achieved experimentally using microstructures (much less than predictions).

There are two theories regarding why increasing the surface area of microelectrodes with microstructures does not result in decreasing impedance as much as expected.

The first theory [48] is that the electrolyte cannot contact the surface in the space between the microstructures.

The second theory [45] is that the resistance of the electrolyte trapped in the narrow space between the microstructures is the limiting factor .This issue will be discussed in the next chapter.

Surface roughness can result in an increase in hydrophobicity (when the liquid cannot lay completely on the surface) and will increase the contact angle of drops on the surface [57].

The contact angle is the angle that a drop of liquid will make with the surface.

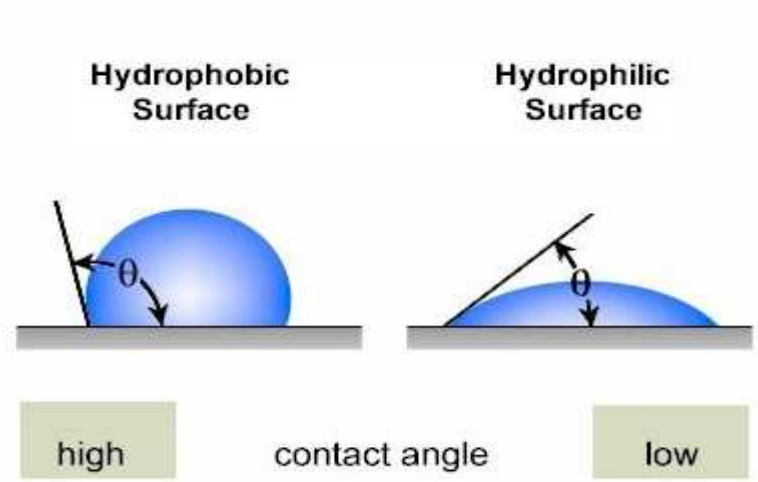

Fig. 23. Contact angle

A drop of liquid can sit on solid microstructures in 2 different ways. See Figure 24.

Cassie and Baxter regime [57]

Wenzel regime [58]

Fig. 24.Cassie-Baxter and Wenzel regimes

For a rough surface in the Wenzel regime, the contact angle (θ) is calculated from this formula [58]:

$$cos\theta = R_f cos\theta_0 \quad (1)$$

θ_0 is the contact angle for smooth surface

R_f is the roughness factor defined as the ratio of solid- liquid area (A_{sl}-actual area) to its projection on a flat surface(A_f-geometrical or apparent area) so $R_f = {A_{sl}}/{A_f}$

Cassie and Baxter extended the Wenzel equation for the condition when the liquid cannot wet the surface completely. In this case the contact angle will be calculated from this formula [57]:

$$cos\theta = cos\theta_0 - f_{la}(cos\theta_0 + 1) \quad (2)$$

f_{la} is fraction of flat geometrical areas of liquid- air interfaces under the drop (ratio of liquid-air area to the whole flat area under the drop).

There have been many discussions regarding the calculation of criteria for predicting the regime the liquid will take on the rough surface (criteria for transition from Cassie-Baxter regime to Wenzel regime).Most researchers tried to calculate the depth that the liquid could intrude into the structures and comparing it with the height of structures to predict the regime the liquid will have on top of the surface.

C. W. Extrand [59] suggested a simple formula to calculate the depth of intrusion for ultralyophobic surfaces assuming the liquid will establish its true contact angles on the sides of microstructures(square pillars).

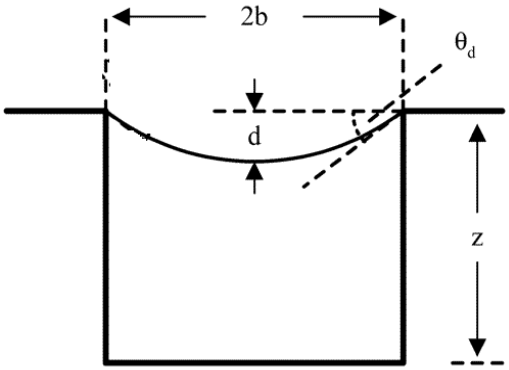

Fig. 25. Depth of water intrusion between microstructures

$$d = btan(\theta_d/2) \qquad (3)$$

Lafuma and Qu´er´e 2003[60] and Nosonovsky and Bhushan 2007 [61] suggested that the curvature would be the same at the top and bottom of the drop because the curvature of the drop depends only on the pressure inside the drop.

Considering $\theta = 40°$ for platinum [62], we can calculate the maximum reduction in impedance for microstructures by calculating the maximum intrusion possible for water (on platinum).

$$cos\theta = cos\theta_0 - f_{la}(cos\theta_0 + 1)$$

$f_{la} = 0.75$ for simple squared top pillars (not checkerboard arrangement-see Fig 14)

$$cos\theta = -0.55 \quad => \quad \theta = 123°$$

$$d = btan(\theta\ /2)$$

so

$$d = btan(123°/2)$$

$$d = b \times 1.84$$

This shows that there can be a limit in the ability of electrolyte to penetrate between the microstructures as we increase the height of them to get the higher aspect ratio and lower impedance. To reduce the impedance of the microelectrode as much as possible it is necessary to have full contact between the solution and microelectrode so the solution should be able to get in between the microstructures. Increasing the distance between the microstructures (*b*) will increase the chance of transition from Cassie and Baxter regime to Wenzel regime for higher aspect ratios (because depth of penetration will be higher) but will decrease the density of microstructures (increase the impedance because of less surface).

To have 100% packing density, pyramidal microstructures must be used. The chance of the solution penetrating between the microstructures is maximum because the distance between the microstructures at the top is maximum for this packing density since they are sharp at the top point [63]. This configuration results in unstable air pockets being formed between the pyramids resulting in good liquid penetration between them.

Chapter 4
Finite Element Analysis

Simulation Parameters

One of the explanations [45] regarding the inability of microstructures to reduce the impedance of microelectrodes was that the resistance of electrolyte trapped in the narrow space between the microstructures was the limiting factor .To test this issue, 2D and 3D simulations have been done using finite element analysis.

The ANSYS [64] finite element analysis software package was used for these investigations. This software solves Poisson's and Maxwell's equations taking appropriate boundary conditions into account. The software divides (meshing) the area or the volume of the materials to small defined shapes (such as bricks, tetrahedral…) called "elements" and solves the equations inside each one of the elements.

To do these simulations, two materials have been identified and modeled for the simulations. These materials are the double layer and the bulk electrolyte (saline).

For each material, the resistivity and permittivity have been defined and then using the software (ANSYS), a simulation has been done to determine the voltage distribution and current. The gain of the microelectrode (factor of impedance reduction over a plane electrode) is calculated as the current that the microelectrode can provide divided by the current that a flat microelectrode can provide.

The double layer has been modeled as a 0.5 nm layer around the surface of the microelectrode as discussed in chapter 1 with:

permittivity= ε_r =6

resistivity= $\rho = R\frac{A}{l} = \frac{R_t \times A}{0.5nm} = \frac{V_t}{0.5nm \times J_0}$

J_0 is the exchange current density for platinum.

Instead of using 0.5nm (5 angstrom) thick structure to represent the interface, a thicker 500nm layer is used instead. The thicker layer allows for more efficient meshing by reducing the size difference between the interface and the electrode geometry [65].

The values for permittivity and resistivity have been changed by the factor of 1000 so that the resulting capacitance and resistance of the double layer remains the same.

Simulations have been done with different layer thickness. Permittivity and resistivity have been changed accordingly and the results remained the same. Thus even though the size of double layer has been increased by different factors, scaling the permittivity and resistivity with the same factor will result in the same answers for the simulation because the resistance and capacitance of the double layer would be the same as before and the current and voltage distribution in bulk electrolyte (where we measure current and voltage) will stay the same. As a further check, a simulation of 20µm microposts was performed and compared with results from the literature [65]. There was no significant difference between the two.

The saline solution has been modeled as the material around the microelectrode and the double layer area, given a size at least 10 times more than microelectrode size.

This means that in Figure 26, the saline solution extends on each side 5 times the microelectrode footprint.

with: permittivity= ε_r =78

resistivity =0.72 Ω-m

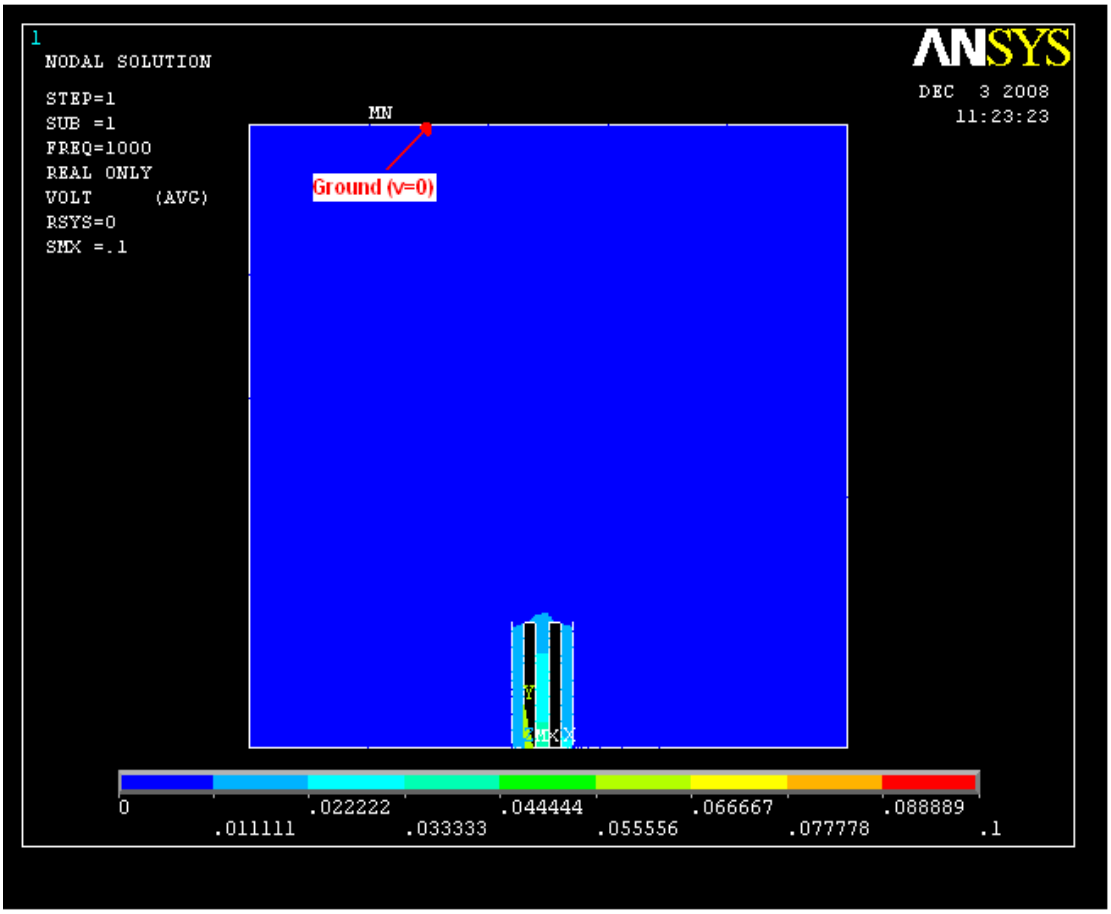

Fig. 26. 2D simulation of platinum electrode with microstructures in saline using Ansys software
Color bar defines range of voltage in the area.

A sinusoidal voltage with the frequency of 1kHz and amplitude of 100mV has been applied to the surface of the microelectrode and the top surface of the saline material in the simulation has been grounded. The simulations have been done for the unit area of a microelectrode. The structures around the unit area have been drawn and simulated to model the same situation in the microelectrode (No voltage has been applied to these structures).

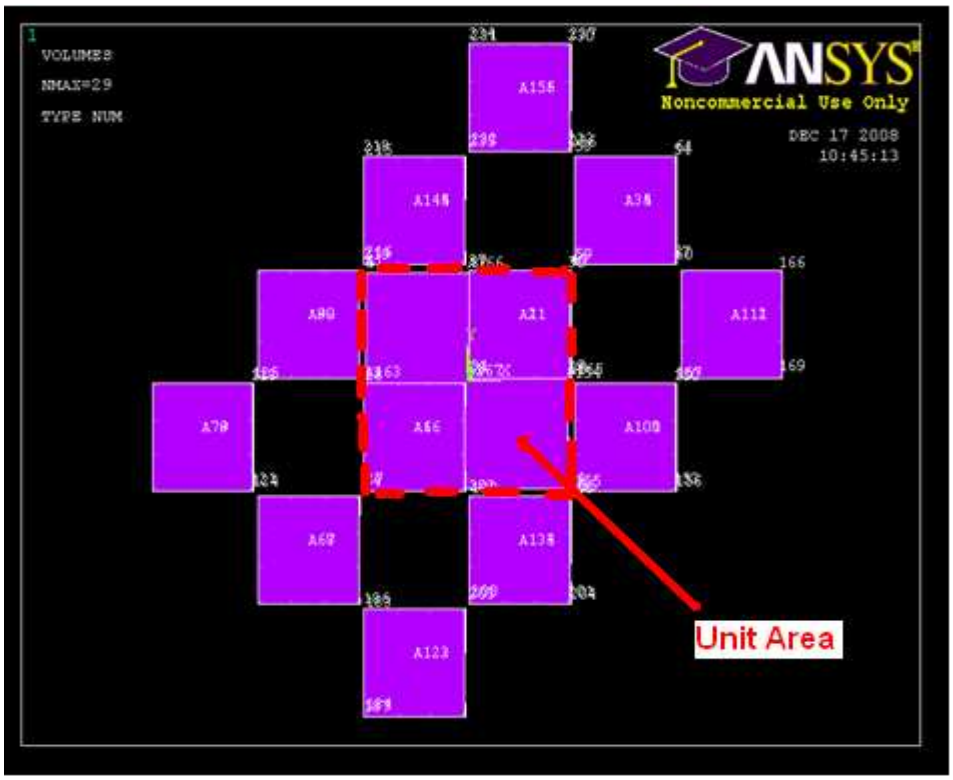

(a)

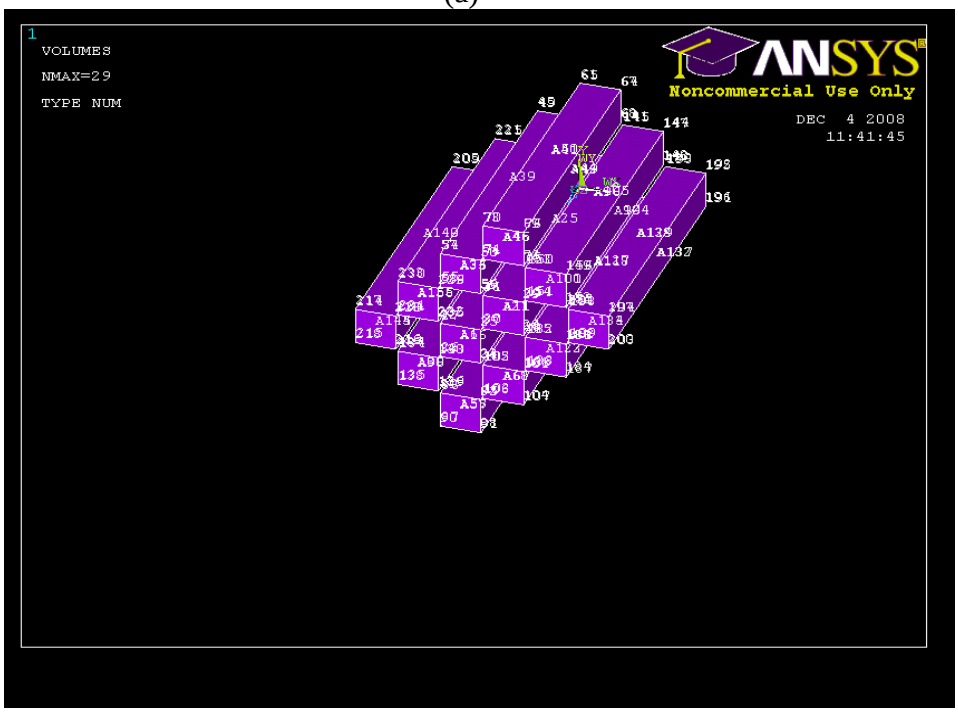

(b)

Fig. 27. Voltage activated unit area in simulation of microelectrode. (a- Top view, b- Side view)

The Simulations have been done for pyramidal structures and squared top pillars.

Results

1- Squared top pillars with different size of unit area. Unit area has been shown for a 3D simulation in Figure 27(The area within the red box). Also see chapter 1 for the definition of unit area.

The results have been shown for w (width of pillar) = 2µm.

- **Gain for simulations (G)**

Gain defined as $\frac{I_{post}}{I_{flat}}$ or the ratio of the current the microelectrode with pillars can provide divided by the current the flat microelectrode can provide for the same voltage applied (frequency of 1kHz and amplitude of 100mV) and this should be the same as the factor of impedance reduction.

$$\frac{Z_{flat}}{Z_{post}} = \frac{V/I_{flat}}{V/I_{post}} = \frac{I_{post}}{I_{flat}}$$

The graphs of these simulations have been shown with letter **"G"** in the legends of the graphs and the number that follows letter "G" is the width of the unit area in micrometers, so for example G6.5 means the simulated factor of impedance reduction when each side of the unit area is 6.5µm.

- **Gain for analytical calculations (g)**

The gain defined as $\frac{A_{post}}{A_{flat}}$ or the area with the pillars to the area of flat microelectrode for graphs of calculations.

This has been calculated as discussed in chapter1 and should be the same factor as the impedance reduction. The graphs of these calculations have been shown with letter **"g"** in the legends of the graphs the number that follows letter "g" is the width of the unit area in micrometer so for example g6.5 means the calculated factor of impedance reduction when each side of unit area is 6.5µm.

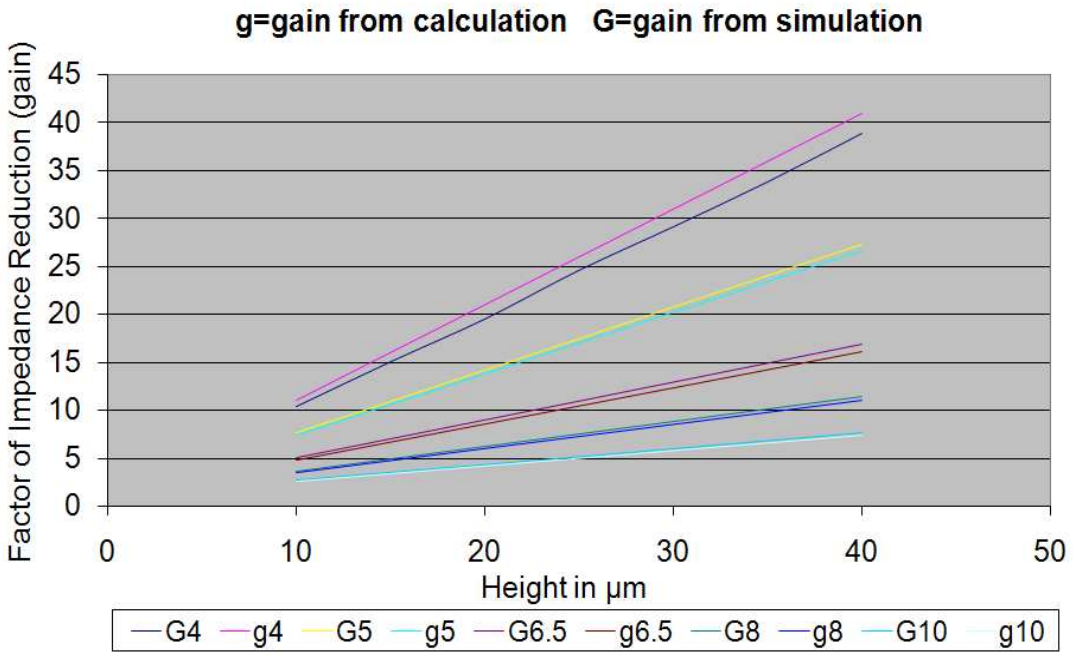

Fig. 28.Gain for different distance between microstructure (square top pillars)

The simulations have shown the same effect of the resistance of electrolyte trapped in the narrow space between the microstructures as has been seen in the literature [45] in particular as the space between the pillars get smaller (smaller unit area).

Yet, though there is some difference between the analytical calculations and the result of simulations for the checkerboard arrangement (the smallest unit area-G4 and g4 in graphs) our simulations show that a factor of reduction in impedance more than one order of magnitude should be achievable but it has not been seen in previous experiments due to air pockets between the pillars.

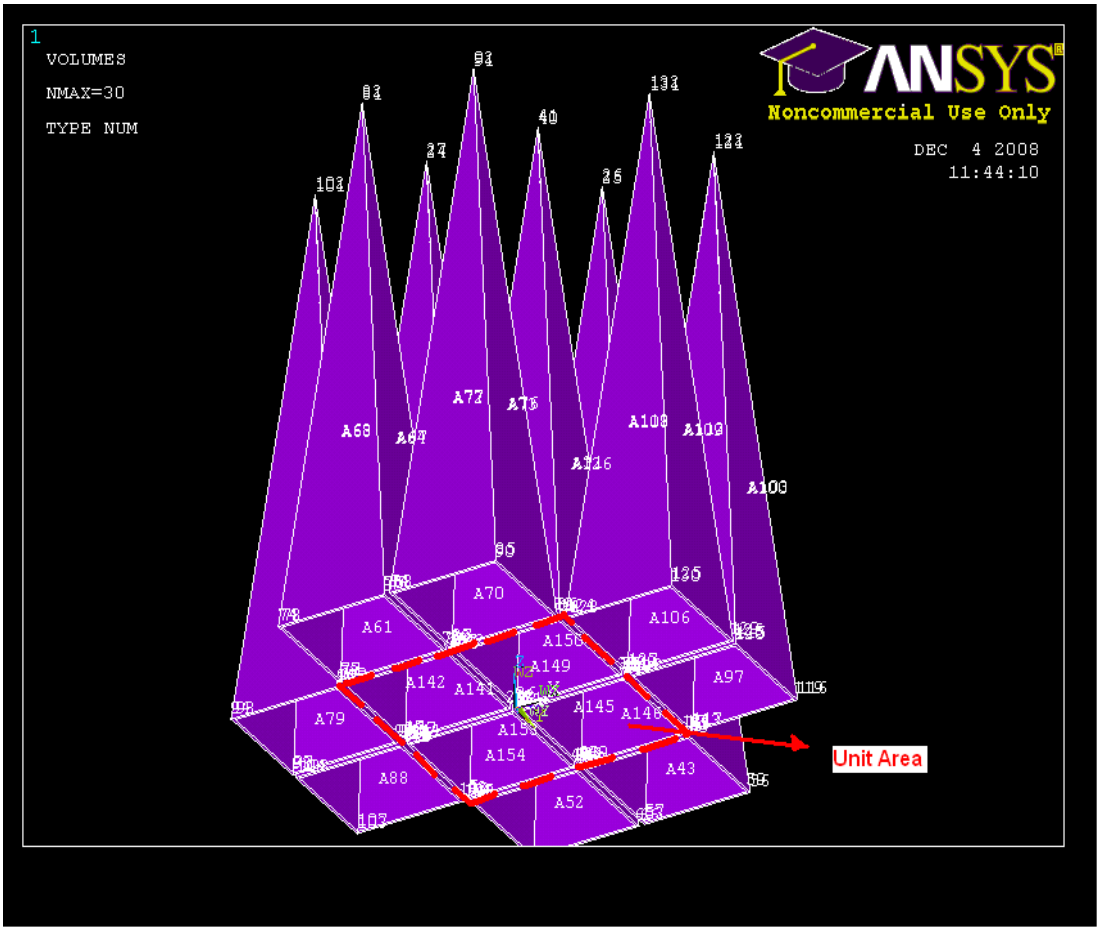

Fig. 29. Pyramids in simulation of platinum electrode using Ansys

The simulation also has been done for pyramidal structures, at highest packing density and that has been compared to the results of simulation for squared top pillars at highest packing density (checker board arrangement).

The width of the base of the structures (pyramidal and pillars) is 2µm.

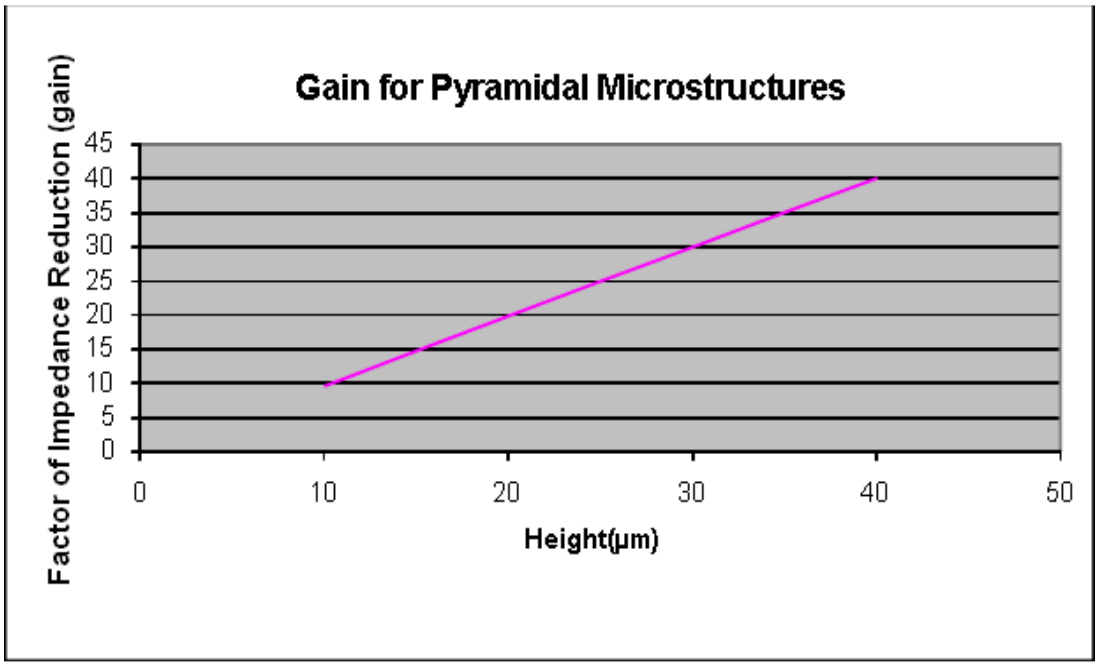

Fig. 30.Gain for Pyramidal structures (results of simulation)

The results show that pyramidal structures can result in reduction of impedance of more than an order of magnitude compared to planar microelectrodes but unlike square top posts there would be less chance for air pockets to be trapped between the posts.

Chapter 5
Analytical Field Calculations and Comparison with Simulation

In this chapter the accuracy of ANSYS simulations for sharp objects will be evaluated to determine the accuracy of the simulations. In finite element analysis the elements around a sharp edge will approximate the sharp edge. The accuracy depends on the size of the mesh of elements and can be a source of error in simulation.

A 2D sharp edge has been simulated and compared with the results of analytical electric field calculations based on electric fields resulting from a sharp hyperbola and a flat ground plate [66].

These calculations are based on defining a conformal [67] transformation that transforms series of lines parallel to the *x*-axis, and in the *z*-plane, to a series of confocal hyperbolas in the *w*-plane.

$$z = x + iy \quad \text{and} \quad w = u + iv$$

$$\textit{transformation: } w = k \cosh z$$

$$k \textit{ is constant}$$

The line $y = \frac{1}{2}\pi$ in the *z*-plane is transformed into the line $u = 0$ in the *w*-plane. A straight line in the *z*-plane, parallel to the *x*-axis and close to it, transforms to a hyperbola in the *w*-plane which corresponds to an idealized edge.

$$u + iv = k \cosh x \cosh iy + k \sinh x \sinh iy$$

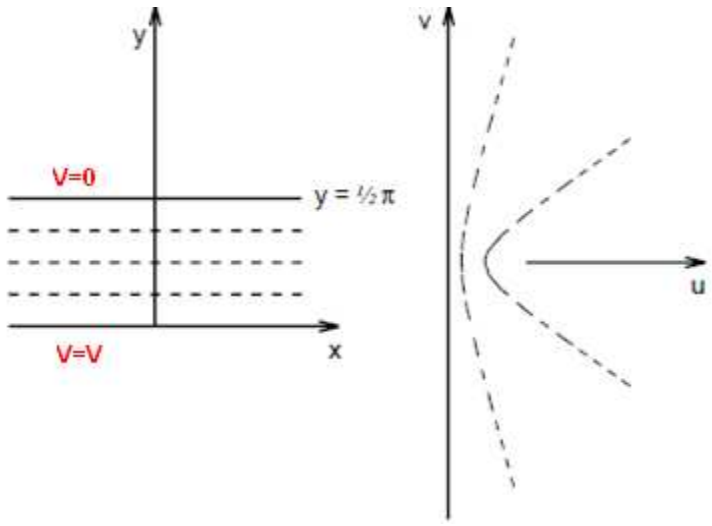

Fig. 31.Transformation of parallel lines to cofocal hyperbolas

The hyperbolas will have these equations:

$$\frac{u^2}{k^2 cos^2 y} - \frac{v^2}{k^2 sin^2 y} = 1\text{Error! Bookmark not defined.}$$

and their asymptotes will be :

$$v = \pm u \tan y$$

The electric field at the intersection of each hyperbola and $v = 0$ is [66]:

$$E_{hyperbola} = -\frac{E_{parallel\ plates}}{ksiny} = \frac{V}{\pi/_2 \times ksiny}$$

So the voltage on each equipotential hyperbola can be calculated by integrating the electric field on $v = 0$

Error! Bookmark not defined.

$$\frac{u^2}{k^2 cos^2 y} = 1 \Rightarrow\ u = kcosy \Rightarrow siny = \sqrt{1 - \frac{u^2}{k^2}}$$

$$V_{hyperbola} = \frac{2V}{\pi}\int_0^u \frac{1}{k\sqrt{1-\frac{u^2}{k^2}}}du = \frac{2V}{\pi}Arcsin(\frac{u}{k})$$

The y=0 axis will be mapped to $v = 0$ with $u > k$ and V=V and y = $\frac{\pi}{2}$ will be mapped to $u = 0$.

Since the sharp edge has to be approximated by a hyperbola, the corresponding equipotential line as the parallel plates should have the same voltage (*V*). So if the approximated hyperbola is corresponding to $y = \beta$ in the parallel plate configurations then the formula for the equipotential hyperbolas will be:

$$V_{hyperbola} = \frac{2V}{\frac{\pi}{2}-\beta}Arcsin(\frac{u}{k})$$

To approximate the sharp edge with a hyperbola these formulas can be used:

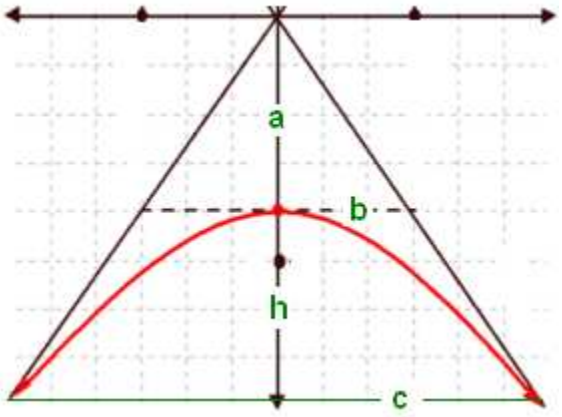

Fig. 32. Hyperbola parameters

The sharp edge sides will be the asymptotes to the hyperbola.

a= The distance between the top of sharp edge to the intersection of hyperbola on the

$v = 0$ axis

b=The distance between the intersection of hyperbola and $v = 0$ and the side of sharp edge (asymptote)

h= The height of sharp edge minus "a"

c=half of the sharp edge's width

$$b = \frac{ca}{a + h}$$

$$\beta = arctg\frac{b}{a}$$

and

$$k = a^2 + b^2$$

The simulation has been done for a sharp edge with ($h = 10\mu m$ and $w = 2c = 2\mu m$ here *h* means the height of sharp edge and *w* is the width) and a sinusoidal voltage has been applied to the sharp edge. The flat plane has been grounded 30µm away from the sharp edge (This was the distance that was needed for the voltage to fall to zero close to 10µm before our actual ground plane.).The difference between the analytical calculations and simulations is that the calculations map an infinite parallel plane to infinitely long hyperbolas, but the simulation is for a sharp edge aspect ratio of 5 ($h = 10\mu m$ and $w = 2c = 2\mu m$) so it is expected that the calculations would be more compatible far away from the sharp edge (because far away the effects of hyperbolic shanks will be negligible) and as the distance from the sharp edge decreases to a value comparable to the height of sharp edge there would be some difference between the calculations and simulation.

The simulation has been done for a sharp edge with $h = 10\mu m$ and $w = 2\mu m$.

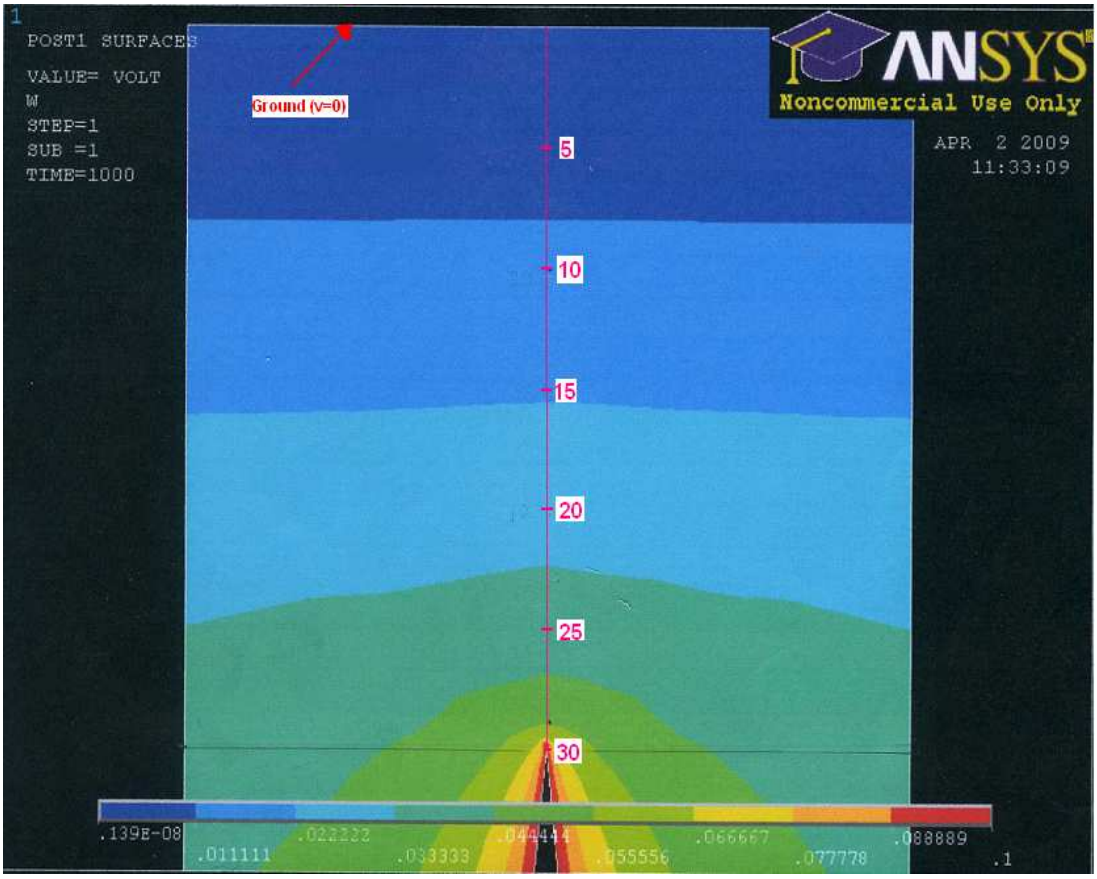

Fig. 33.Simulation of sharp edge equipotential lines *h=10μm*

The values for voltage have been calculated for every 5μm from the ground plane to the sharp edge and have been compared to the results of simulation.

Table IV
Comparison of calculated and simulated voltage at different distances from the ground plane for a sharp edge (h=10μm)

Distance from ground plane	Calculated voltage	Result of simulation (range)
5	0.010829	0-0.011111
10	0.021977	0.011111-0.022222
15	0.03386	0.011111-0.022222
20	0.047188	0.022222-0.033333
25	0.063696	0.033333-0.044444
30	0.099947	0.088889-0.1

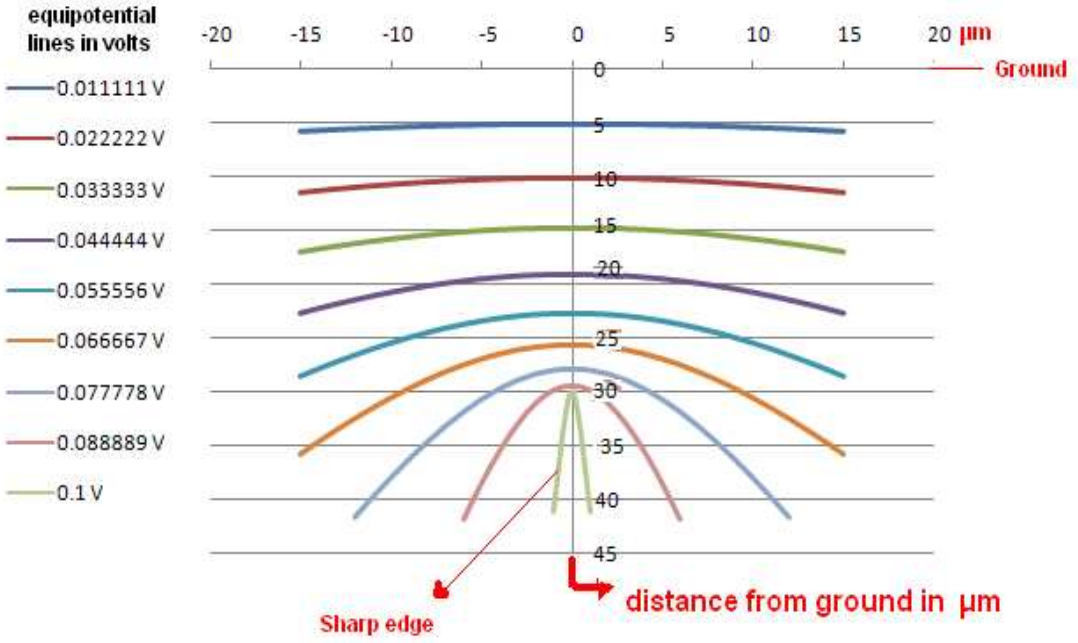

Fig. 34.The results of calculation of sharp edge equipotential lines

If the height of the sharp edge is increased, (taper angle constant and equal to the angle of original sharp edge with 10µm height and 2µm width) the results will be more compatible with the calculations. Therefore the simulation has been done for a sharp edge with $h = 30\mu m$ (see Figure 35).

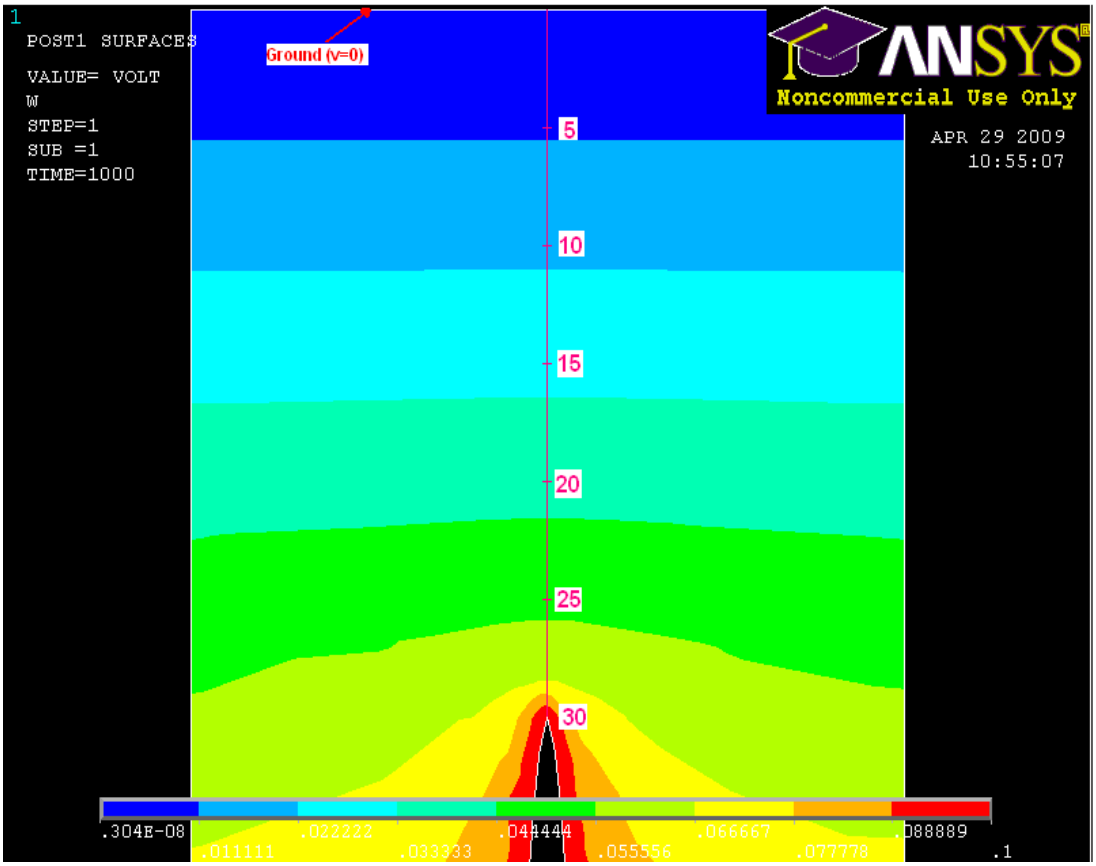

Fig. 35.Simulation of sharp edge equipotential lines h=30µm

Table V
Comparison of calculated and simulated voltage in different distances from the ground plane for a sharp edge (h=30µm)

Distance from ground plane	Calculated voltage	Result of simulation(range)
5	0.010829	0-0.011111
10	0.021977	0.011111-0.022222
15	0.03386	0.022222-0.033333
20	0.047188	0.033333-0.044444
25	0.063696	0.044444-0.055556
30	0.099947	0.088889-0.1

Table VI
Comparison of calculated (infinite height) and simulated equipotential lines for sharp edges (h=30μm) and h=10 μm)

Voltage (equipotential lines)	Calculated distance from ground plane	Simulated distance h=10μm	Simulated distance h=30μm
0.011111	5.127307256	8	5.533981
0.022222	10.10373429	16.85714	11.06796
0.033333	14.78284082	22.28571	15.14563
0.044444	19.02693571	26.57143	21.5534
0.055556	22.71143187	28.85714	25.92233
0.066667	25.72724484	29.42857	28.54369
0.077778	27.98598746	29.57143	29.12621
0.088889	29.42119217	29.71429	29.41748

It can be seen from Table VI that by increasing the height of the sharp edge the calculation and simulation will be more compatible. Figure 36 shows the simulations of sharp edges with *h=30μm and h=10μm* and analytical calculations together with obvious more compatibility between *h=30μm* and calculations.

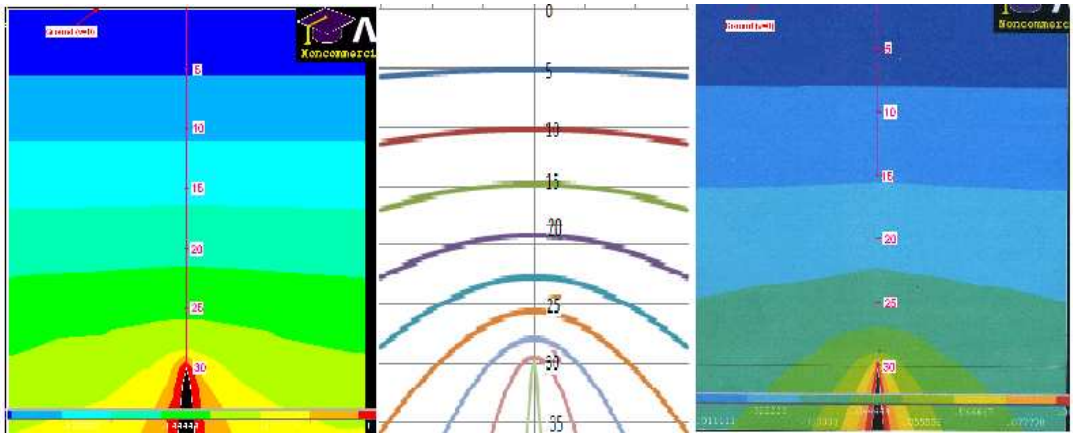

(a) (b) (c)

Fig. 36. Comparing simulation and calculations
(a) Simulation of sharp edge equipotential lines h=30µm
(b) Calculation of sharp edge equipotential lines
(c) Simulation of sharp edge equipotential lines h=10µm

This shows that the result of simulations for a sharp edge is close to the results of analytical electric field calculations for the same sharp edge so one can be confident that a sharp edge simulation will be accurate.

Chapter 6
Design and Fabrication

To test the idea of whether making pyramidal microstructures on microelectrodes will reduce their impedance more than what is shown in the literature, a fabrication plan has been designed. Commercial microelectrodes for biomedical applications have been obtained from Ayanda biosystems (Qwane Biosciences). These microelectrodes were made of platinum and SU8 as the insulator with 5µm thickness. Each electrode has a diameter close to 30µm.The impedance of these microelectrodes is normally around 1MΩ.

The fabrication process has two steps:

1-Electroplating the microelectrodes (a-c)

- a- Original microelectrode
- b- Electroplating
- c- Microelectrode after complete electroplating

2-Creating microstructures using Focused ion beam patterning (d)

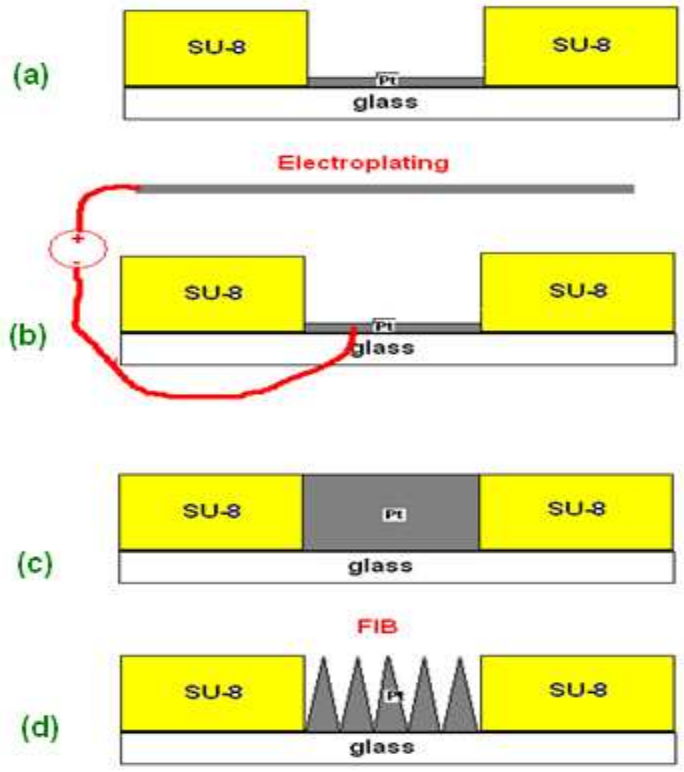

Fig. 37.Fabrication processes of pyramidal microstructures on microelectrodes
a) Original microelectrode
b) Electroplating
c) Microelectrode after complete electroplating
d) Creating microstructures using Focused ion beam

Electroplating

Electroplating is a process in which metal ions in a solution are moved by an electric field to coat an electrode. The process uses electrical current to reduce cations of a desired material from a solution and coat a conductive object with a thin layer of the material, such as a metal. The part to be plated is the cathode (negative) of the circuit.

The anode (positive) is made of the metal that will be plated on the part. Both components are immersed in a solution called an electrolyte containing one or more dissolved metal salts as well as other ions that permit the flow of electricity. A power supply supplies a current to the anode, oxidizing the metal atoms so they will dissolve in the solution. At the cathode, the dissolved metal ions in the electrolyte solution are reduced at the interface between the solution and the cathode, and they "plate out" onto the cathode [68].

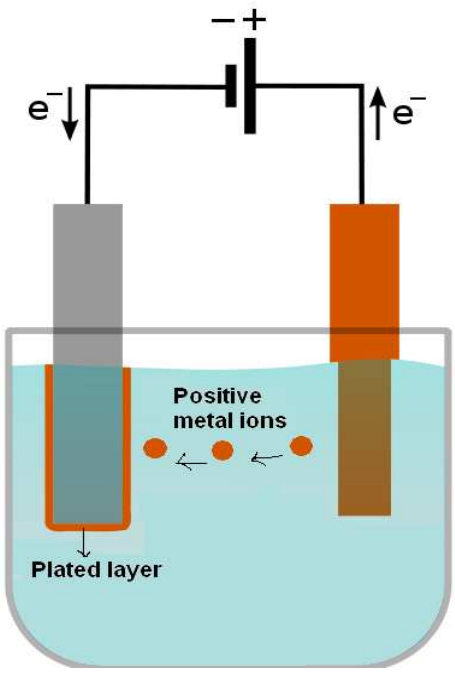

Fig. 38.Electroplating

In our case the cathode was the electrodes. The anode was platinum wire (obtained from Surepure Chemetals, USA).To decrease the impedance of the anode the platinum wire has been wrapped around itself in the shape of a coil (increasing the

area). The solution or electrolyte was Platinum Diammine Dinitrite (P Salt) and Ammonium Sulfamate (from Technic Inc., USA).

In electroplating, a negatively charged layer is formed around the cathode as the process continues. When using DC, this layer charges to a certain thickness and obstructs the ions from reaching the part. To solve this problem in practice, the output is sometimes periodically turned off to cause this layer to discharge somewhat. This allows easier passage of the ions through the layer and onto the part on which we wish to plate [69].

The other advantage of this technique is that high current density areas in the bath become more depleted of ions than low current density areas. During OFF time, ions migrate to the depleted areas in the bath. When pulse ON occurs, more evenly distributed ions are available for deposition onto the part we wish to plate [69].

The problem with electroplating the microelectrodes was that not all of the microelectrodes would have the same thickness of platinum electroplated on them and in some cases platinum starts to come out of the hole (in the SU8) and spreads on the SU-8 before filling up the hole (see Fig. 40b) similar to the electrode plating that has been reported in other experiments [44].

To reduce this problem, pulse plating has been chosen because of the capability of plating more evenly [69]. The power supply has been set to provide 2 volts for 90 seconds and 0 volt for 10 seconds. The microelectrodes have been connected to each other (15 of them on one side of the microelectrode array) and electroplated.

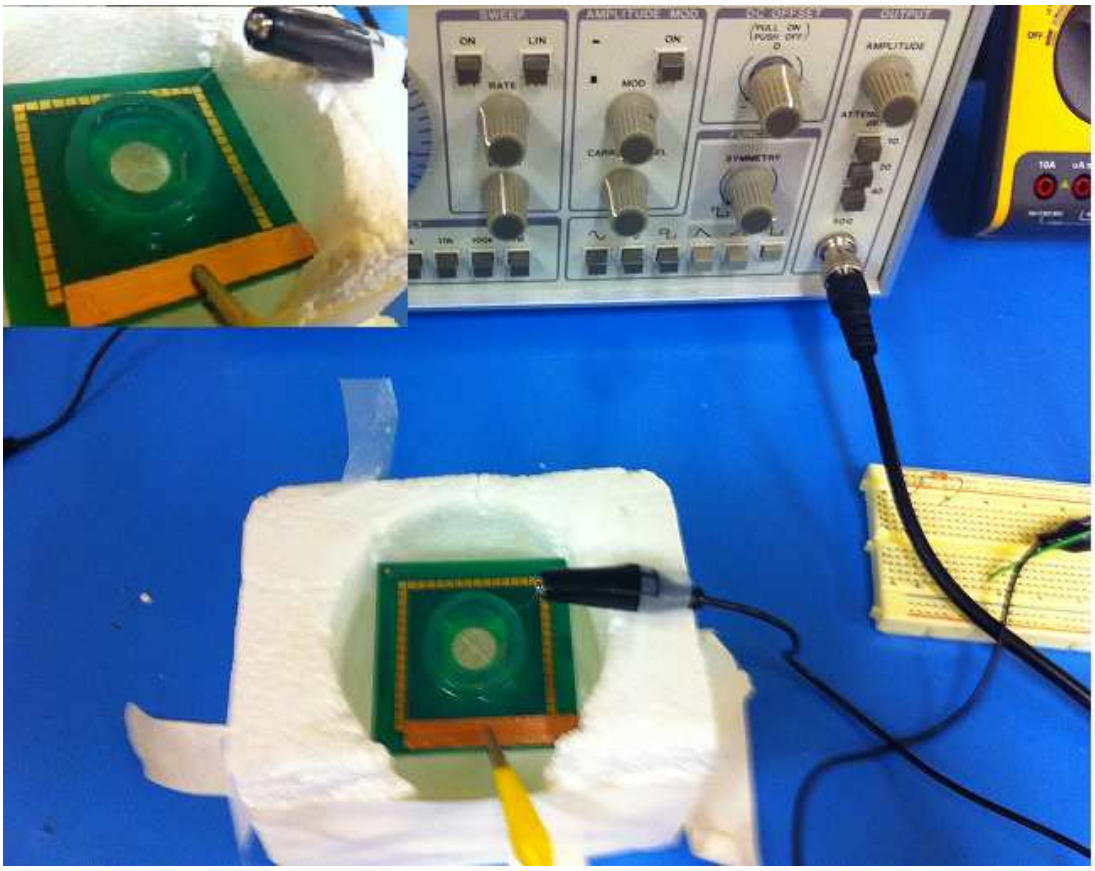

Fig. 39.Platinum electroplating of microelectrodes

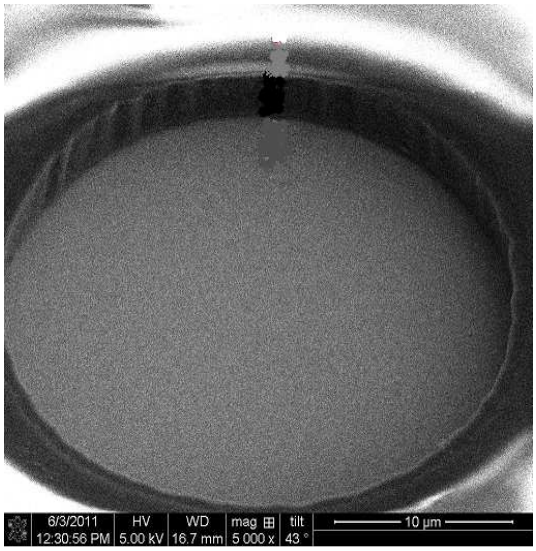

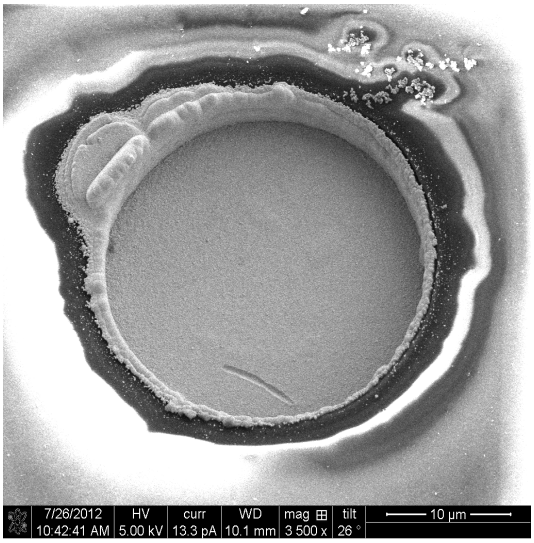

(a) Before Electroplating **(b) After Electroplating**

Fig. 40.Microelectrode Before and After electroplating

FIB

Focused ion beam, also known as FIB, is a useful technique in the semiconductor industry and materials science. FIB has also some applications in the biological field as it can provide the ability of three dimensional morphology and precise sectioning [70a].

The FIB machine is a scientific instrument that looks a lot like a scanning electron microscope (SEM). However, while the SEM uses a focused beam of electrons to image the sample the FIB uses a focused beam of ions instead. FIB machines can also have both electron and ion beams, allowing the sample to be investigated using either of the beams [70b].

Almost all FIB machines are using liquid-metal ion sources (LMIS), especially gallium ion sources [70b] because of low melting point which minimizes interdiffusion with tungsten needle and also heavy mass. Ion sources based on elemental gold and iridium are also available [71] although such sources are not commonly used due to their expense and other problems.

In ion source part of a FIB machine, gallium metal is placed in contact with a tungsten needle and the needle is heated to near evaporation, gallium wets a sharp heat resistant tungsten needle with a tip radius of 2-5μm and flows to the tip of the needle where the opposing forces of surface tension and electric field form the gallium into a cusp shaped tip called a Taylor cone [70b]. The apex of this cone is very small (~5 nm) in diameter.

The intense electric field at the small tip causes ionization and field emission of the gallium atoms (created by an electrode called extractor just under the needle).

Source ions are then generally accelerated and focused onto the sample by electrostatic lenses.

The primary ion beam hits the sample surface, the collisions of the incident ions with the surface create secondary ions and secondary electrons which are collected to form an image of the surface as the beam is rastered across the surface [70b].Secondary electron detection is the chief method of imaging but images can be obtained using back-scattered electrons or secondary ions as well which are more useful in studying the material structure of the sample.

In summary we have these main parts in a FIB machine:

• **Electron / Ion source**

The beam of electrons or ions is emitted from this part with selectable energy.

• **Lens system**

The beam enters the lens system consisting of several electromagnetic lenses (for electron beams) or electrostatic lenses (for ion beams because they are heavier) and exits to hit the specimen surface.

• **Scan unit**

The scan generator moves the beam in a raster over the specimen area using deflection plates or scan coils.

• **Detection unit**

The detector system picks up the ions or electrons, converts them into an amplified electrical signal which is then sent to the control computer and displayed on the monitor.

The entire electron path from source to specimen must be under vacuum so that the particles do not collide with air molecules.

There are two ways of creating microstructures using FIB machines and these are either milling or gas assisted deposition. In milling, high energy ions impact the material and shape the surface by removing the material. In deposition, a gaseous compound is introduced through fine gas nozzles close to the surface of the sample. The ion beam will decompose the gas into volatile and nonvolatile parts and nonvolatile parts will stay on the surface and will create the deposition [70c].

Chemical analysis has shown that platinum deposited in this fashion contains a large amount of carbon incorporated into it from the broken down precursor gas (30–50%) [72] and deposits usually show higher resistance than expected for pure platinum. This is the main reason for choosing milling over platinum deposition in this project.

To create a pattern using milling, a bit map file can be used to tell the machine how much milling is needed in each spot (pixel).

For the FEI Quanta 3D dual beam [73] which was used in this project, each pixel in a 24 bits RGB bitmap file consists of:

• The **Red** component – currently not used.

• The **Green** component – determines if the beam is blanked. Any other value than 0

activates the beam.

• The **Blue** component – determines the dwell time per pixel. If blue is set to 0 the dwell

time of a pixel is 100 ns. If blue is set to 255 the maximum dwell time is used.

The dwell time for the pixels in between these values is linearly interpolated and then rounded to the value from a (fixed) dwell time table with 124 entries.

The beam current in this project was 3nA at 30kV.The beam current is directly related to the spot size of the beam which in this case will be ideally 66nm in diameter according to the machines manual. It is important for the pattern's pixel size to be greater than beam diameter.

Dwell time is the time that the beam spends in each spot. To estimate the dwell time needed to make pyramids with the highest aspect ratio possible, for each microelectrode a hole has been made to measure the thickness of platinum and the dwell has been determined based on that. The measurements in the machine are based on a simple calibration on a regular grid of known dimensions so the machine will count the pixels on the image between two chosen spots and based on the calibration calculates the distance.

When the sample is tilted by angle θ, there are two tilt correction modes, surface and cross-section. Surface is for measuring features parallel to the surface, and it divides the apparent horizontal length by cos(θ) to give the actual length along the surface. Cross-section is for measuring features perpendicular to the surface, like the holes, and it divides the apparent horizontal length by sin(θ) to give the real depth of the

feature. Measurements that have been cross-section corrected are denoted by "cs" on the images.

The pattern that was chosen to make pyramidal microstructures is designed to make pyramids with 1µm width. The pattern will be 11× 11 pixels so each pixel will have the size of $\frac{1\mu m}{11}$ or 91nm which is bigger than beam diameter. The pattern for one pyramid has been shown in Fig. 41. The pattern is 11 × 11 pixels. The middle pixel is red which means blue and green is set to “0”. This is the very top of pyramid in which no milling will be done. For the rest of the pixels, green has been set to “1” and blue has been changed from “0” to “1” in five steps (shades) which means more milling as the pixel goes from yellow to white (red is set to “1” everywhere but has no effect).The value for steps one and two are both “0” because it has been observed that without this change, the height of the post will be cut shorter probably because the beam has a gaussian distribution and the overlap of the beam for neighboring pixels at the top will result in milling the top.

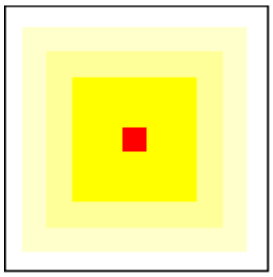

Fig. 41. The pattern for one pyramid

Several of the pyramid patterns have been put together in a circle to be transferred to the microelectrode as shown in Fig.42.

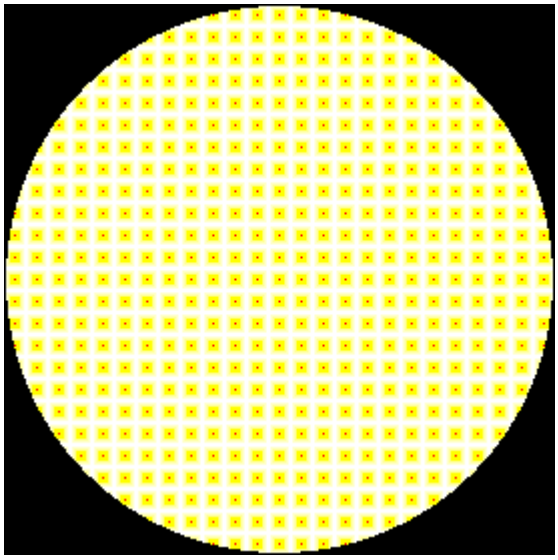

Fig. 42. Complete pattern of microelectrode

It has been observed that drift in the beam position (possibly due to impact with other molecules in the vacuum chamber and also the charging up of SU-8 around the microelectrodes and other contaminants on the surface of the microelectrode) can be a problem for making the pattern, so the vacuum in the chamber should be of the order of 10^{-5} mbar. Also to reduce the effect of drift on the pattern the "maximum dwell time" has been increased (based on the height of pyramids) so that pyramids can be made in one pass of the beam. The height of the pyramids is the same as the thickness of the platinum coat on the microelectrode. To estimate this thickness and

determining the maximum dwell time, a hole has been made on the microelectrode and the thickness has been measured (Figure 43).

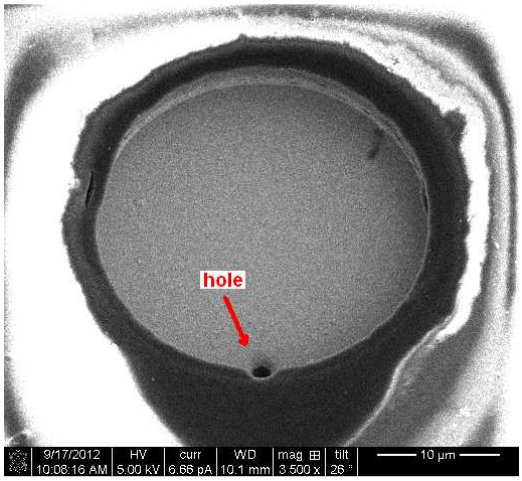

Fig. 43. A hole in microelectrode to measure the thickness

Fig. 44 shows the effects of the drift on the pattern when it is made in one pass. The pattern was supposed to cover the surface of microelectrode but instead it was roughly ¾ of the diameter. The diameter of the microelectrode is 30µm and the time to finish the pattern was 10 minutes which means the drift was around $\frac{30}{4\times10\times60}$ = 12.5 nm/s (downward).

The drift also creates some misshaped pyramids during the process and some of the pyramids are thicker and many of them have extra roughness on their surfaces. Some pyramids also came out shorter than the rest.

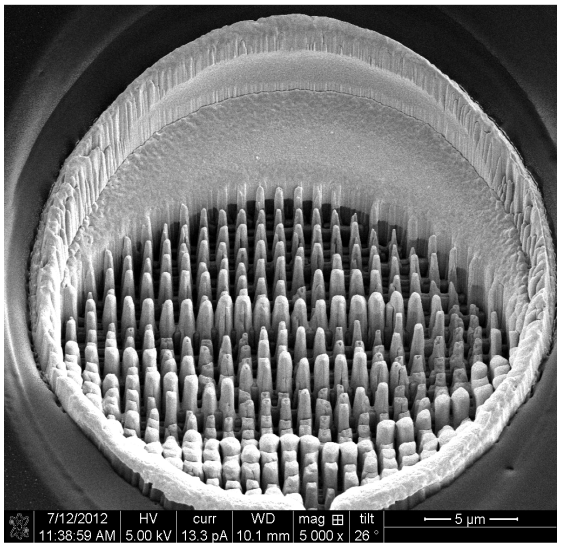

Fig. 44. The effects of drift on the pattern

Also for those microelectrodes with extra platinum spreading around the hole due to electroplating, FIB has been used to clean around the hole (see Fig. 45) .

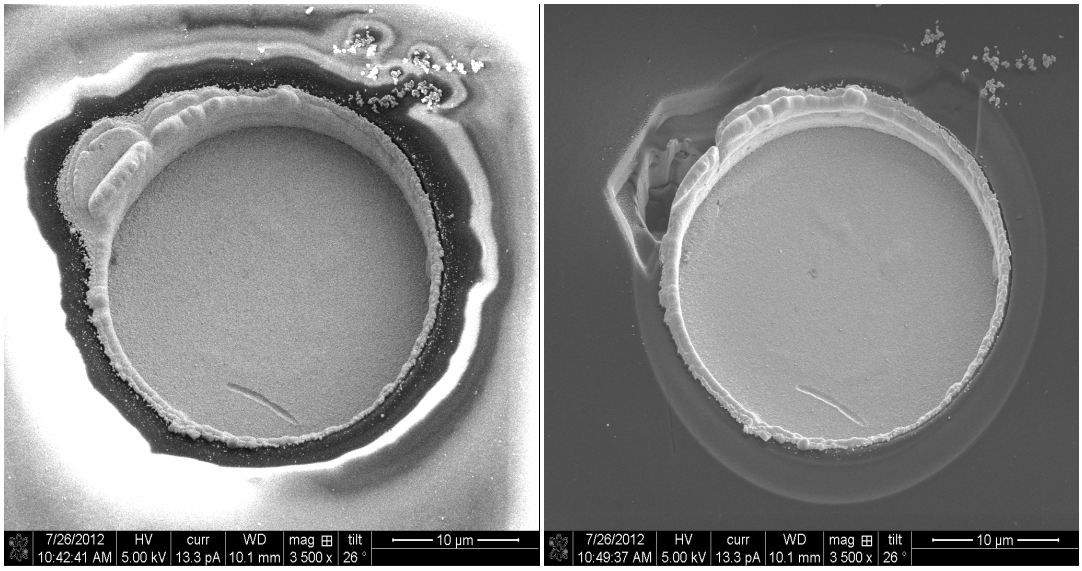

(a) Before Cleaning **(b) After cleaning**

Fig. 45. Microelectrode Before and After cleaning

Fig. 46. shows few samples of microelectrodes at the end of the process and Fig. 47. shows close up of microstructures.

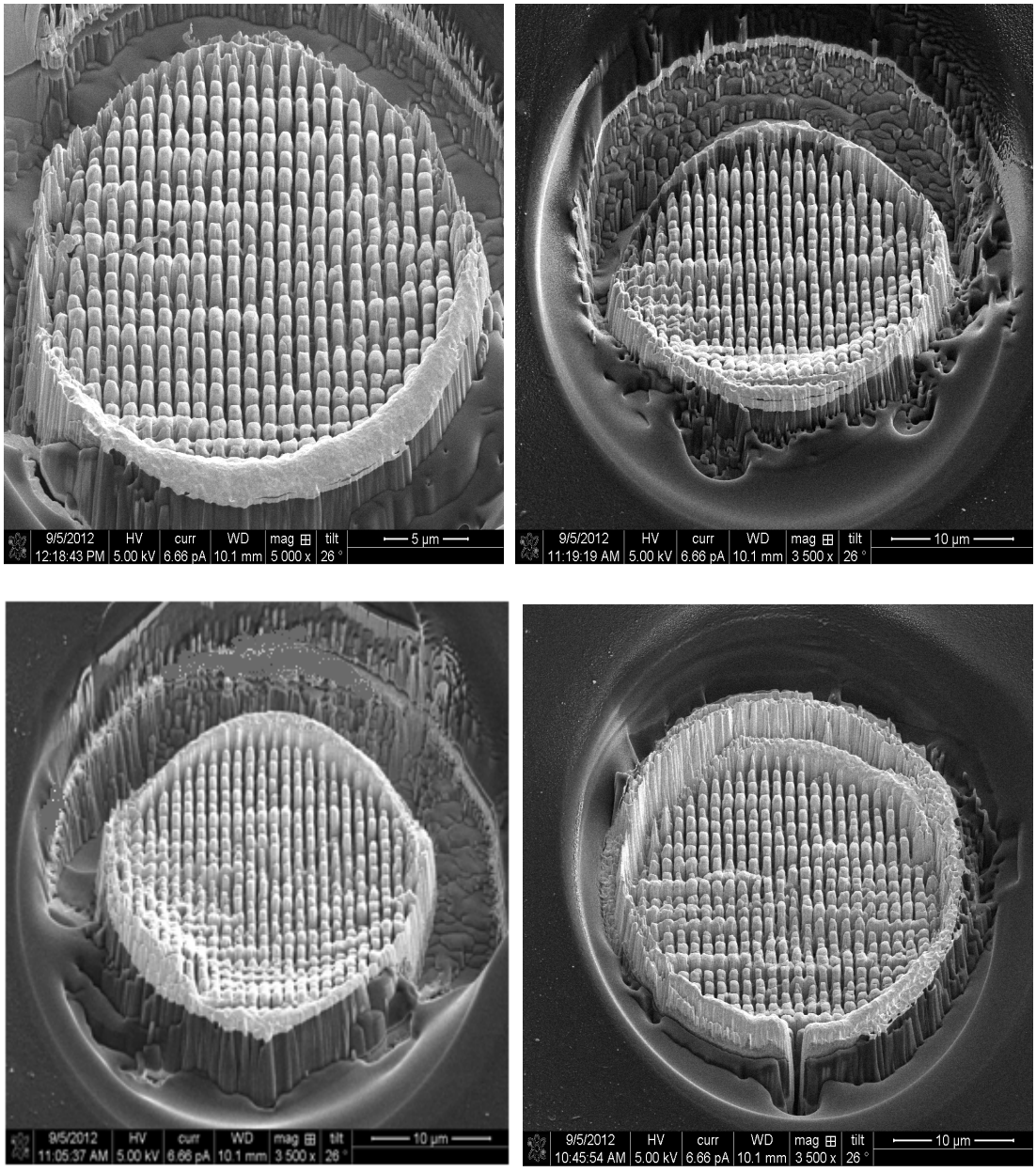

Fig. 46. Samples of microelectrodes at the end of process

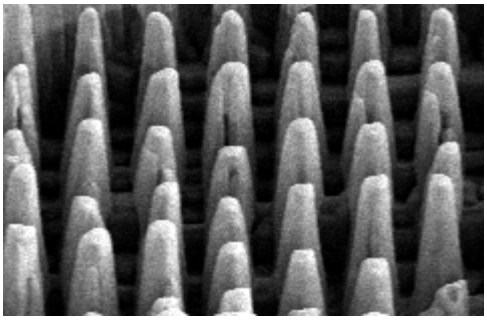

Fig. 47. Close up of microstructures

The area shown is 7µm×4µm.Each microstructure is 1µm×1µm at the base

Ga and Toxic Considerations

Since in this study, the FIB uses Focused Gallium ions for milling, there is the possibility of some gallium ions getting implanted into the platinum. This can raise a question about the level of toxicity of Gallium on cells. Gallium has shown to have low level toxicity on cells to the point that it has been considered as a replacement for mercury in dental amalgam [74].

It has been reported that concentration of gallium ions around cells up to 1mmol/L was safe and no cytotoxic effects have been noticed.[74]

$$1\,mmol\ /\ L\ =\ 6.02\times 10^{20}\ ion\ /\ L\ =\ 6.02\times 10^{17}\ ion\ /\ cm^{3}$$

Gallium ions will be implanted in platinum with a gaussian distribution shown below [75]:

$$N(x) = N_{\max}\ \exp\left[-\frac{1}{2}\left(\frac{x - R_p}{\Delta R_P}\right)^2\right]$$

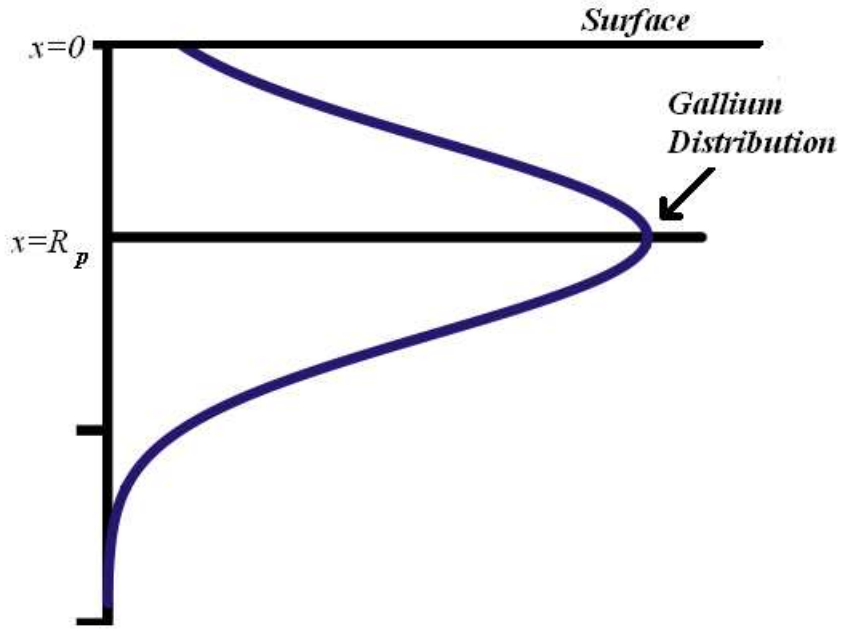

Fig. 48. Guassian distribution of implanted Gallium

x is the distance from the surface of material exposed to gallium ion beam. $N_{\max}$ is the maximum concentration of penetrated Gallium ions which will happen at distance R_P from the surface.

$N_{\max}$ is proportional to the dose of ions that will be sent toward the sample. R_P is the average range of penetrated ions projected on the direction of the incident and ΔR_P is its standard deviation which can be calculated as [75]:

$$\Delta R_P = \frac{2R_p\sqrt{M_1 M_2}}{3(M_1 + M_2)}$$

and

$$R_P = \frac{R}{1+(\frac{M_2}{3M_1})}$$

R is the average range of penetrated ions (not projected). M_1 and M_2 are ions atomic mass and substrate atomic mass respectively so the concentration of Gallium on the surface (x=0) can be calculated as:

$$N(0) = N_{\max} \exp[-\frac{1}{2}.(\frac{3(M_1 + M_2)}{2\sqrt{M_1 M_2}})^2]$$

For Gallium M_1=69.72 and Platinum M_2=195.08 the concentration of Gallium on the surface will be:

$$N(0) = N_{\max} e^{-5.8}$$

$N_{\max}$ is proportional to the dose of ions but in the worst case there would be a layer of Gallium at R_P .Gallium has atomic radius of 135 pm so a layer of Gallium will not have more than $(\frac{10^{-2}}{2 \times 135 \times 10^{-12}})^2 = 1.37 \times 10^{15}\ ion/cm^2$ which means on the surface there will be no more than

$1.37 \times 10^{15} \times e^{-5.8} = 4.14 \times 10^{12}\ ion/cm^2$.

If all these ions break the bonds with platinum and are released around the neurons, considering the smallest neurons will not be less than 1 μm , then the worst concentration of gallium around the neurons will be less than

$\frac{4.14 \times 10^{12}}{10^{-4}} = 4.14 \times 10^{16}\ ion/cm^3$

This is an order of magnitude less than the safe concentration reported in the literature [74].

Chapter 7
Measurements and Results

Impedance Measurement

The impedance of a microelectrode is usually determined by measuring the voltage and current of the microelectrode while it is in the solution. A power supply is needed to create current. The measurement is done in a circuit consisting of the microelectrode we are interested in measuring its impedance (usually it is called working electrode) and another electrode which is necessary for the closing loop of our circuit (reference electrode) [9].

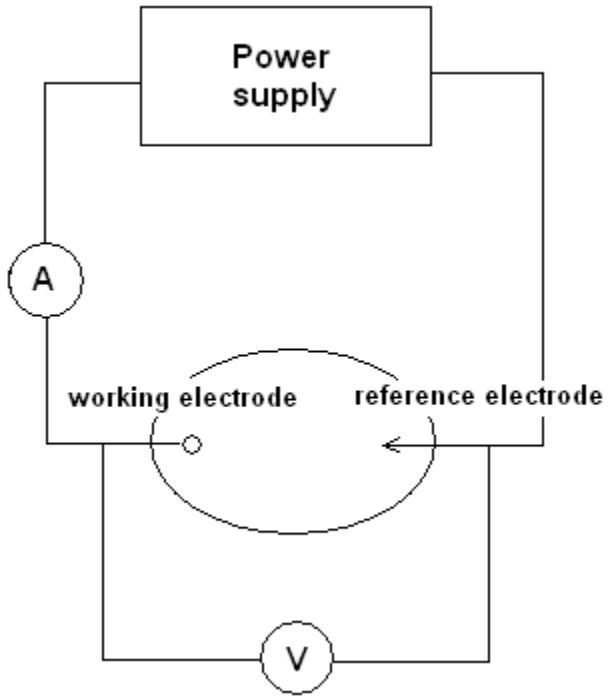

Fig. 49. Two electrode cell

This arrangement is called a “2 electrode cell” and is useful only if the reference electrode is made with very large area (low impedance) compared to the working electrode because what is measured in this arrangement is actually the impedance of the working electrode plus the impedance of the reference electrode and the solution.

The other arrangement which is usually used in more accurate measurements is the “3 electrode cell”. In this arrangement we have the working electrode, another electrode which is called the counter electrode or auxiliary electrode and a reference electrode which in this case will measure the working electrode voltage.

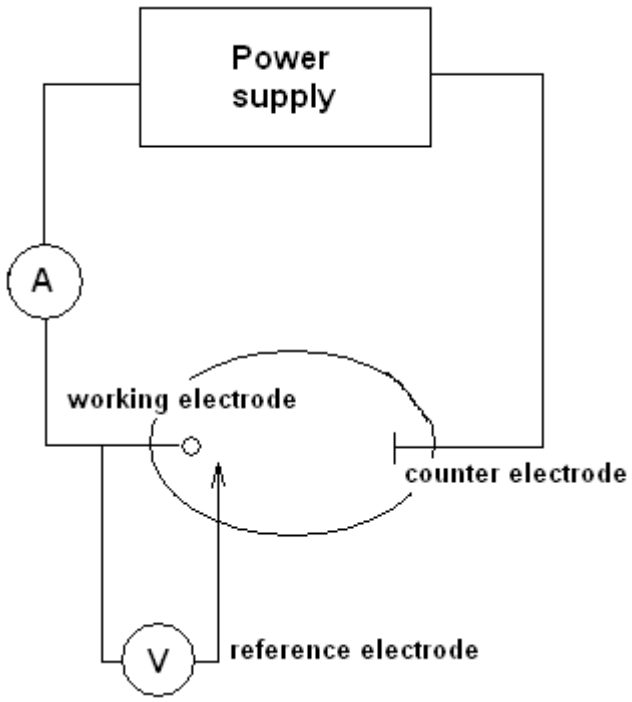

Fig. 50. Three electrode cell

In this project we used the “2 electrode” configuration because the microelectrodes are small (30µm diameter) and the impedance is in the range of 1MΩ and the solution resistance can be calculated as:

$$R_s = \rho / 4r = \frac{0.72}{4 \times 15 \times 10^{-6}} = 12K\Omega \quad \text{(see chapter one)}$$

So the solution resistance compared to the microelectrode resistance (about 1MΩ) is negligible.

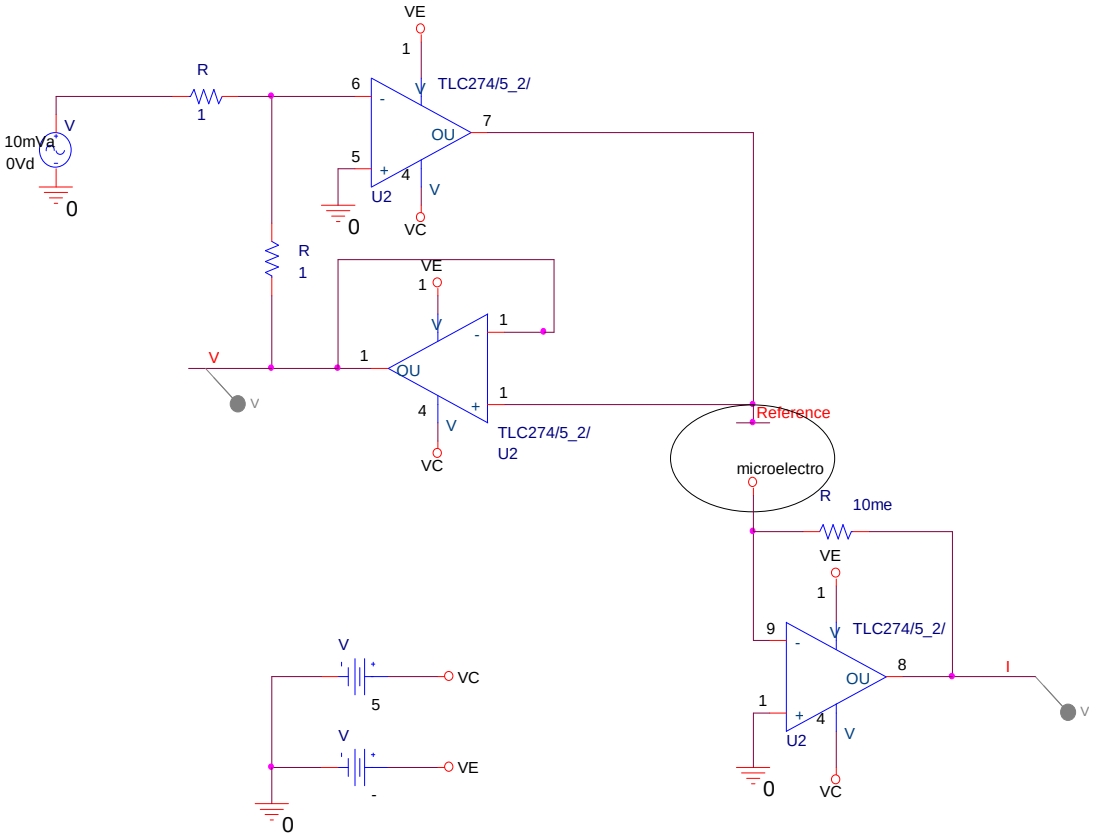

Fig. 51.Potentiostat design for 2 electrode cell

The op-amp is TLC274BCN which is a general purpose op-amp with high input impedance and low noise necessary for measuring high impedances because it is

important that the input impedance of the op-amp does not interfere with the microelectrode impedance in the measurement circuit. Since we are working with 10mv signals to measure the impedance (to keep the microelectrode impedance in neural recording mode-see chapter 1) a low noise op-amp is desired. The circuit in Fig. 51.has been used in this project to measure the impedance of microelectrodes. Microelectrodes have also been tested with a Gamry Reference 600 [76] potentiostat machine with no significant difference in the results.

Results

44 Microelectrodes on 4 different sets of microelectrode arrays have been electroplated and patterned. The results of the impedance measurements have been given in table VII.

The impedance of microelectrodes has been measured before the start of the process and their impedances have been found to be between 700KΩ and 1MΩ which is the same as what the manufacturer claims. In Table VII the impedance of the microelectrode before the process has been calculated as 1MΩ for simplification purposes (Z_B). The gain after each step (i.e. Electroplating or FIB) is calculated as "Impedance before process" over "Impedance after that step of the process". The reduction in impedance after electroplating depends on the roughness of the electroplated coat and is not controllable or repeatable but the average gain in reduction of impedance increases with the thickness of the coat.

To calculate the reduction in impedance by creating the pyramidal microstructures, the formulas for calculating the area of a pyramid can be used and the gain can be

calculated as the area of pyramid over the area of the base. In This case the width of the base is 1µm so the area of the base is 1µ²m.The area of the pyramid can be calculated as:

$$Area = 2\sqrt{h^2 + 0.25}$$

Also since during electroplating, platinum tends to cover the walls of the 5µm deep hole of SU-8, this has to be considered too. The area of the wall is:

The perimeter of the microelectrode × 5µm thickness of the wall = $30\pi \times 5$ = 471.24µ²m

The area of the microelectrode is$15 \times 15 \times \pi = 707\mu^2 m$. This means there will be an extra gain of impedance reduction equal to the ratio of the area of the wall and the area of the microelectrode. The extra gain can be calculated as: $\frac{471.24}{707} = 0.67$.

So the total gain can be calculated as:

$$gain = 2\sqrt{h^2 + 0.25} + 0.67$$

Table VIII shows the results of calculation versus the results of impedance reduction after electroplating and after the FIB process. It seems that the results of measurement at the end of the process regarding the factor of impedance reduction (gain) are roughly twice as what was expected considering the calculations (see Table VIII). This can be a result of misshapes of pyramids and extra roughness on the surface of them. The extra roughness provides even more area and therefore less impedance.

Fig. 52 shows misshapes and roughness of the surface of microstructures.

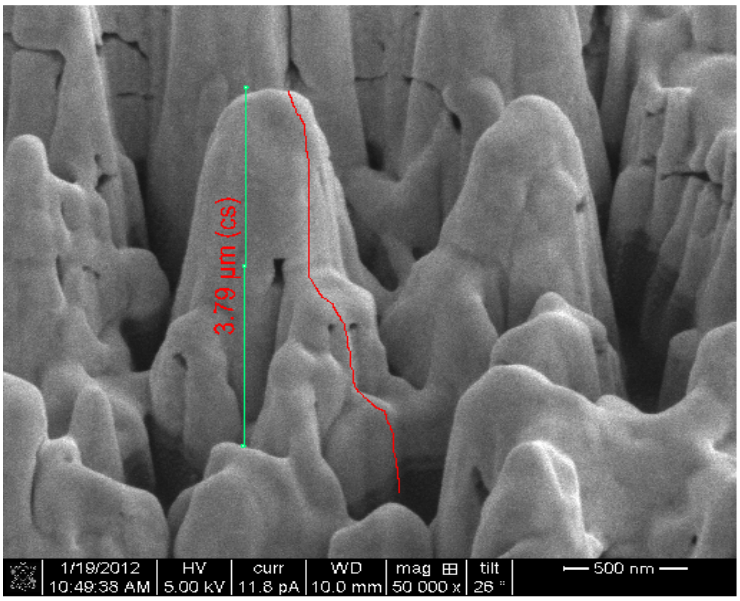

Fig. 52. Misshapes and extra roughness of the microstructures

Table VII
Results of the impedance measurements in different steps of process
(All impedance values are in KΩ, $Z_B = 1000K\Omega$)

Sample	Impedance after Electroplating (Z_E)	Gain after Electroplating ($\frac{Z_B}{Z_E}$)	Impedance after FIB (Z_F)	Gain after FIB ($\frac{Z_B}{Z_F}$)	Height of microstructures in µm
S4B2	500	2	142.8	7	1
S4L1	1000	1	166.6	6	1
S4R9	250	4	142.8	7	1.5
S4T14	500	2	125	8	1.5
S2T5			100	10	2
S3T6	166.6	6	90.9	11	2
S4L5	1000	1	105.2	9.5	2
S2T2	125	8	80	12.5	3
S2T3	125	8	80	12.5	3
S3B10	500	2	100	10	3
S3R1	125	8	76.9	13	3
S5B11	100	10	80	12.5	3
S5B9	111	9	83.3	12	3
S5L10	400	2.5	125	8	3
S5L11	333.3	3	125	8	3
S5L13	333.3	3	86.9	11.5	3
S5L7	400	2.5	153.8	6.5	3
S5L9	333.3	3	117.6	8.5	3
S5R12	125	8	80	12.5	3
S5R14	142.8	7	83.3	12	3
S5R4	142.8	7	83.3	12	3
S5R5	125	8	83.3	12	3
S5T15	200	5	83.3	12	3
S3R6	71.4	14	50	20	3.5
S5L3	100	10	66.6	15	3.5
S5T14	153.8	6.5	62.5	16	3.5
S2T4	142.8	7	57.1	17.5	4
S2T7	142.8	7	57.1	17.5	4
S3R14	71.4	14	55.5	18	4
S3R2	71.4	14	52.6	19	4
S3R9	66.6	15	38.4	26	4
S5R6	111	9	55.5	18	4
S5T8	125	8	57.1	17.5	4

Table VII
Results of the impedance measurements in different steps of process (Continue)
(All impedance values are in KΩ, $Z_B = 1000K\Omega$)

Sample	Impedance after Electroplating (Z_E)	Gain after Electroplating ($\frac{Z_B}{Z_E}$)	Impedance after FIB (Z_F)	Gain after FIB ($\frac{Z_B}{Z_F}$)	Height of microstructures in µm
S3B1	44.4	22.5	31.25	32	5
S3B12	125	8	68.9	14.5	5
S3B4	55.5	18	44.4	22.5	5
S3B7	83.3	12	62.5	16	5
S3R12	57.1	17.5	43.4	23	5
S3R3	66.6	15	52.6	19	5
S3R4	62.5	16	47.6	21	5
S3R7	50	20	40	25	5
S5T9	125	8	57.1	17.5	5
S3R13	44.4	22.5	28.5	35	6

Table VIII
Comparison of measurements and calculations of impedance reduction

Height of Microstructures in µm	Calculated Gain ($\frac{Z_B}{Z_F}$)	Average Gain after Electroplating ($\frac{Z_B}{Z_E}$)	Average Gain after FIB ($\frac{Z_B}{Z_F}$)	Range of gain after FIB
1	2.9	1.5	6.5	6-7
1.5	3.8	3	7.5	7-8
2	4.7	3.5	10.1	9.5-11
3	6.7	5.8	10.9	8-13
3.5	7.7	10.1	17	15-20
4	8.7	10.5	19	17.5-26
5	10.7	15.9	22.5	16-35

The Factor of impedance reduction using this technique is at least 5 times more than what has been achieved previously in the literature also there is potential for even

more impedance reduction since the commercial microelectrodes that have been obtained had a 5µm SU-8 layer and thus that was the maximum electroplating thickness achievable.

There is a lot of potential for improving this technique in using thicker insulation layers and achieving even higher aspect ratios which will result in less impedance.

Conclusions

Different theories regarding modeling of microelectrodes and also neuron cell bodies have been studied and summarized so one can simulate the results of recording from real live neuron from intracellular generation to the output of amplifier.

Advantage and disadvantage of metal microelectrodes and FET based sensors for neural recordings has been discussed.

Different ways of reducing the impedance of the microelectrode and their problems regarding their stability especially for long term implantable devices has been presented. The problems with designing low impedance microelectrodes by creating microstructures have been discussed in detail and calculations and simulations have been done to define the origins of problems.

Finally based on our calculations and simulations a plan has been defined to design low impedance microelectrodes with higher stabilities for in vivo applications. The fabrication process has two parts which consist of first electroplating the microelectrodes and then creating microstructures using focused ion beam patterning. Milling has been chosen over deposition to create microstructures because FIB

depositions are not pure and usually show higher resistance than expected for pure platinum.

A bitmap pattern has been designed to make pyramidal microstructures. The pattern will define the milling time in each pixel for the machine. To create the pyramid there will be no milling at the top and more milling it goes toward the sides so the pixels will go from darker shades to lighter shades as we go toward the sides. Several of the pyramid patterns have been put together in a circle to be transferred to the microelectrode.

Drift was the main problem in transferring the pattern on to the microelectrode and creating microstructures. To reduce the effect of drift on the pattern the “maximum dwell time” has been increased so that pyramids can be made in one pass of the beam. Since gallium ions will be implanted into the platinum, calculations have been done to ensure that the final product will not have toxic effects on cells.

The Impedance of commercial microelectrodes has been reduced more than 1 order of magnitude with a simple procedure and the mechanical stability and impedance of these microelectrodes are better than what has been reported in the literature. This technique can potentially have many applications for implantable biomedical microelectrodes where impedance and mechanical stability of microelectrodes are both important.

There is also a lot of potential for improving this technique in regards to improving impedance reduction by making higher aspect ratio microstructures and also improving in making the procedure more repeatable by controlling the drift in FIB

machine. One way of controlling the drift can be designing a sacrificial layer with another layer of metal on top of the SU-8 isolation layer. This layer will be removed after creating the microstructures but will be grounded during FIB process and prevents SU-8 from charging up and deflecting the beam. This plan has been shown in Fig. 53.

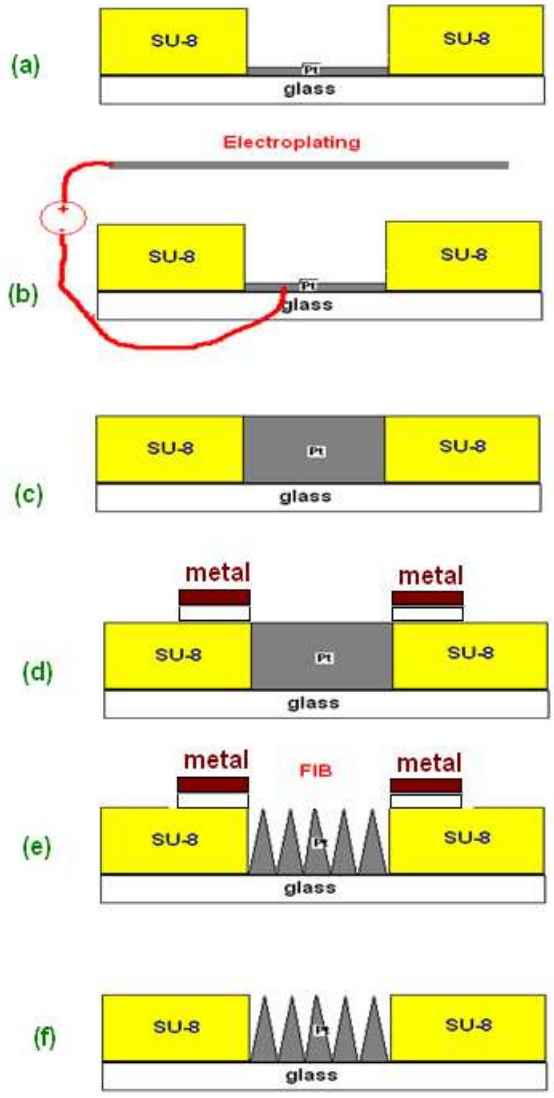

Fig. 53. Fabrication processes with sacrificial metal layer

References:

1- Daniel R. Merrill, Marom Bikson, John G.R. Jefferys “Electrical stimulation of excitable tissue: design of efficacious and safe protocols” *Journal of Neuroscience Methods, Volume 141, Issue 2, pp. 171–198, 15 February, 2005*

2- J. D. Weiland, D. J. Anderson, and M. S. Humayun, "In vitro electrical properties for iridium oxide versus titanium nitride stimulating electrode", *IEEE Trans. Biomed. Eng., vol. 49, no. 12, pp.1574 -1579, 2002*

3- D. B. McCreery, W. F. Agnew, T. G. H. Yuen and L. A. Bullara, “Comparison of neural damage induced by electrical stimulation with faradaic and capacitor electrodes” *Annals of Biomedical Engineering, Volume 16, Number 5 ,pp. 463-481, 1988*

4- A. Seger, E. de Asis, W. K. Wong, L. Wang, K. Kagoo, J. Hieb, M. Isaacson, C. Y. Yang “Characterizing Neuronal Networks Using Carbon Nanotube Microelectrode Arrays”, *Proceedings of the 3rd International Congress of NanoBiotechnology & Nanomedicine, 2006, June 19-21, San Francisco*

5- Paolo Bonifazi, Peter Fromherz, “Silicon Chip for Electronic Communication Between Nerve Cells by Non-invasive Interfacing and Analog-Digital Processing” *Advanced Materials, vol. 14, No.17, September 3, 2002*

6- Peter Fromherz, “Nanoelectronics and Information Technology” Rainer Waser, Ed. , *Berlin: Wiley-VCH, 2003, pp.781-810*

7- G. Kovacs, “Microelectrode models for neural interface” in *Enabling Technologies for Cultured Neural Networks*. David A. Stenger, Thomas M. McKenna, Ed. San *Diego, CA: Academic Press, 1994, ch.7, pp. 121-165.*

8- David A. Robinson, “The Electrical Properties of Metal Microelectrodes”, *Proceedings of the IEEE, vol. 56, No 6, June 1968.*

9- A. J. Brad and L. R. Faulkner “Electrochemical Methods” *New York: Wiley, 1980.*

10- John O'M. Bockris, Amulya K.N. Reddy, “Modern Electrochemistry”, *Volume 2 Plenum Press, New York,1970*

11- E. Warburg “Ueber das verhalten sogenannter unpolarisirbarer elektroden gegen wechselstorm.” *Ann. Phys. Chem. vol. 67, pp. 493-499, 1899.*

12- E. Warburg “Ueber die polarisationcapacitat des platins.” *Ann. Phys. vol. 6, pp.125-135, 1901.*

13- J.Newman “Resistance for flow of current to a disk.” *J. Electrochem. Soc. 113, vol. 5, pp. 501-502, 1966.*

14- M. Becker “Heat Transfer” *New York: Plenum, 1986.*

15- D.J. Edell, V.M. Mcneil, L.D. Clark. “Microfabrication technology for development of chronic neural information transducers.” *Technical Digest—International Electron Devices Meeting. New York: IEEE Press, pp. 180–3, 1986.*

16- T. Sakurai and K. Tamaru “Simple formulas for two-and three-dimentional capacitances.” *IEEE Transaction on Electron Devices, ED-30(2), 183-185, 1983.*

17- R. C. Gesteland, B. Howland, J. Y. Lettvin, and W. H. Pitts, “Comments on microelectrodes”, *Proc. IRE, vol. 47, pp. 1856-1862, November 1959.*

18- E. T. McAdams, A. Lackermeier, J. A. McLaughlin & D. Macken "The linear and non-linear electrical properties of the electrode-electrolyte interface" *Biosensors & Bioelectronics 10, pp. 67-74, 1995.*

19- H. Fricke, "The theory of electrolyte polarization", *Philosophical Mag.*, vol. 7, *pp.310- 318, 1932.*

20- R. De Levie, "The influence of surface roughness on electrochemical measurements." *J. Electrochem.Soc., 107, pp.113-130, 1965.*

21- M. Kramer, & M. Tomkiewicz, "Porous electrodes 1: Numerical simulation using random network and single-pore models". *J. Electroch. Soc., 131(6), pp.1283-1288, 1984.*

22- S.H. Liu, "Fractal model for the AC response of a rough interface." *Phys. Rev. Lett., 55, pp. 529-532, 1985.*

23- J.C. Wang & J.B. Bates, "Model for the interfacial impedance between a solid electrolyte and a metal electrode." *Solid State Ionics, 12-19, pp. 224-228, 1986.*

24- Conrad D. James, Andrew J. H. Spence, Natalie M. Dowell-Mesfin, Rifat J. Hussain, Karen L. Smith, Harold G. Craighead, Michael S. Isaacson, William Shain, and James N. Turner, "Extracellular Recordings From Pattered Neural Networks Using Planar Microelectrode Arrays", *IEEE Transaction on Biomedical Engineering, vol. 51, No 9, September 2004.*

25- B.B. Mandelbrot, "The Fractal Geometry of Nature." *New York: Freeman, 1983.*

26- E.T. McAdams, “Effect of surface topography on the electrode-electrolyte interface impedance. Part 3. The fractal approach.” *Surface Topography,*3, 3-24, *1990.*

27- L. F. Richardson “The problem of contiguity: an appendix of statistics of deadly quarrels”, *General Systems Yearbook 6, pp.139-187, 1961.*

28- Jens Feder, Torstein Jøssang and Einar Rosenqvist “Scaling Behavior and Cluster Fractal Dimension Determined by Light Scattering from Aggregating Proteins”, *Phys. Rev. Lett. 53, pp.1403 – 1406, October 1984.*

29- Dale W. Schaefer, James E. Martin, Pierre Wiltzius and David S. Cannell “Fractal Geometry of Colloidal Aggregates”, *Phys. Rev. Lett. 52,pp. 2371 – 2374, June 1984.*

30- R. F. Voss, R. B. Laibowitz, and E. I. Allessandrini “Fractal (Scaling) Clusters in Thin Gold Films near the Percolation Threshold” *Phys. Rev. Lett. 49, pp.1441 - 1444, November 1982.*

31- B. Sapoval, “Fractal electrodes and constant phase angle response: Exact examples and counter examples.” *Solid State lonics, 23, pp.253-259, 1987.*

32- L. Nyikos, & T. Pajkossy, “Fractal dimension and fractal power frequency-dependent impedance of blocking electrodes.” *Electrochim. Acta.,* 30(11), *pp.1533-1540, 1985.*

33- Wendy Franks, Iwan Schenker, Patrik Schmutz and Andreas Hierlemann “Impedance Characterization and Modeling of Electrodes for Biomedical

Applications", *IEEE Transaction on Biomedical Engineering, vol. 52, No 7, July 2005.*

34- Piet Bergveld "New Amplification Method for Depth Recording", *IEEE Transaction on Biomedical Engineering, vol. BME-15, No 2, April 1968.*

35- Wen-Yaw Chunga, Chung-Huang Yang a,b, Dorota G. Pijanowskac, Piotr B. Grabiec d, Wladyslaw Torbicz c, "ISFET performance enhancement by using the improved circuit techniques", *Sensors and Actuators B: Chemical, 2005.*

36- Chou Jung-Chuan, Hsiao Ching-Nan, "Drift behavior of ISFETs with a-Si: H-SiO2 gate insulator", *Materials Chemistry and Physics vol. 63, No 3, pp. 270-273, March 2000.*

37- Luc Bousse, Piet Bergveld, "The Role of Buried OH Sites in the Response Mechanism of Inorganic-Gate pH-Sensitive ISFETs" *Sensors and Actuators, pp 65 – 78, 1984.*

38- Manfred Klein, **"**Time Effects of Ion-Sensitive Field-Effect Transistors", *Sensors and Actuators, 17, pp. 203 – 208, 1989.*

39- Behzad Razavi, "Design of Analog CMOS Integrated Circuits" *New York: McGraw-Hill, 2001.*

40- Yannis P. Tsividis, "Operation and Modeling of the MOS Transistor", *Second ed.,Boston: McGraw-Hill,1999.*

41- C. Jakobson, I. Bloom and Y. Nemirovsky "1/*f* Noise in CMOS transistors for analog applications from subthreshold to saturation", *Solid-State Electronics, vol. 42, Issue 10, pp. 1807-1817, October 1998.*

42- C. A. Marrese “Preparation of strongly adherent platinum black coatings.” *Anal. Chem.* ***59****(1), pp.217-218, 1987.*

43- G. E. Loeb, R. A. Peck, J. Martyniuk “Toward the ultimate metal microelectrode.” *Journal of Neuroscience Methods, vol.63, no.1-2, pp.175-83, Dec. 1995. Publisher: Elsevier, Netherlands.*

44- Andy Hung, David Zhou, Robert Greenberg, and Jack W. Judy, “Micromachined Electrodes for High Density Neural Stimulation Systems”, *IEEE Micro Electro Mechanical Systems Workshop (MEMS 2002), Las Vegas, Nevada, pp. 56-59, January 20-24, 2002.*

45- S. Bauerdick, C. Burkhardt, D.P. Kern and W. Nisch “Substrate-Integrated Microelectrodes with Improved Charge Transfer Capacity by 3-Dimensional Micro-Fabrication”,*Biomedical Microdevices, Volume 5, Number 2, June, 2003.*

46- A. Hung, D. Zhou, R. Greenberg, J.W. Judy “Dynamic simulation and testing of the electrode-electrolyte interface of 3-D stimulating microelectrodes.” *2005 2nd International IEEE/EMBS Conference on Neural Engineering (IEEE Cat. No.05EX938). IEEE 2005, pp. 179-82. Piscataway, NJ, USA.*

47- A. Hung, D. Zhou, R. Greenberg, J.W. Judy “Micromachined electrodes for retinal prostheses.” [*Conference Paper] 2nd Annual International IEEE-EMBS Special Topic Conference on Microtechnologies in Medicine and Biology. Proceedings (Cat. No.02EX578). IEEE 2002, pp. 76-9. Piscataway, NJ, USA.*

48- K. Wang “A Carbon Nanotube Microelectrode Array for Neural Stimulation.” *PHD thesis,Stanford University,2006*

49- http://employees.csbsju.edu/hjakubowski/classes/ch331/signaltrans/olsignalneuron.html

50- Harvey Lodish ... [et al.], "Molecular cell biology" *New York: W.H. Freeman, 4th ed, chapter 15 and 21, 2000.*

51- Constance Hammond "Cellular and molecular neurobiology" *San Diego, Ca: Academic Press, chapter6, 1996.*

52- http://www.neuron.yale.edu/neuron/

53- http://genesis-sim.org/

54- S. Vassanelli, P. Fromherz "Neurons from rat brain coupled to transistors**."** [Journal Paper] *Applied Physics A (Materials Science Processing), vol.65, no.2, pp. 85-88, Aug. 1997. Publisher: Springer-Verlag, Germany*.

55- J. E. B. Randles "Kinetics of rapid electrode reactions" *Discussions of the Faraday Society* **1,** *1947.*

56- http://www.cadence.com/products/orcad/pspice_simulation/pages/default.aspx

57- A. Cassie and S. Baxter "Wettability of Porous Surfaces" *Trans. Faraday Soc. **40** 546–5 51, 1944.*

58- R. N. Wenzel "Resistance of solid surfaces to wetting by water" *Ind. Eng. Chem. **28** 988–994, 1936.*

59- C. W. Extrand "Criteria for Ultralyophobic Surfaces" *Langmuir, 20 (12), pp. 5013–5018, 2004.*

60- A. Lafuma and D. Qu´er´e "Superhydrophobic states" *Nat. Mater. **2**, pp. 457–460, 2003.*

61- M. Nosonovsky and B. Bhushan “Hierarchical roughness optimization for biomimetic superhydrophobic surfaces” *Ultramicroscopy **107**, pp. 969–979, 2007.*

62- A. Adamson, A. Gast “Physical Chemistry of Surfaces” *New York: John Wiley & Sons, 1997, pp. 365.*

63- Bhushan B, Yong Chae Jung. “Wetting, adhesion and friction of superhydrophobic and hydrophilic leaves and fabricated micro/nanopatterned surfaces.” [*Journal Paper] Journal of Physics: Condensed Matter, vol.20, no.22, pp. 225010 (24), 4 June 2008. Publisher: IOP Publishing Ltd., UK.*

64- http://ansys.com/

65- Andy Hung, David Zhou, Robert Greenberg, and Jack W. Judy, ,”Dynamic Electrochemical Simulation and Testing of Micromachined Electrodes for Neural Stimulation”, *Proceedings of the Seventh International Symposium on Electrode Processes and Physical Electrochemistry, 206th Meeting of the Electrochemical Society (ECS 2004)*, Honolulu, Hawaii (October 3-8, 2004).

66- David F. Brailsford and Andrew J. B. Robertson, “Calculation of Electric Field Strengths at a Sharp Edge “*International Journal of Mass Spectrometry and Ion Physics, 1., pp. 75-85, 1968.*

67- Ervin Kreyszig, “Advanced Engineering Mathematics” *New York: John Wiley &Sons, Fourth ed., 1979.*

68- Fredrick A. Lowenheim “Modern Electroplating” *New York: John Wiley &Sons, Second ed., 1963.*

69- M.S. Chandrasekar, Malathy Pushpavanam “Pulse and pulse reverse plating—Conceptual, advantages and applications” *Electrochimica Acta 53, pp. 3313–3322, 2008.*

70a-Kirk Hou and Nan Yao “Applications for biological Materials” in Focused Ion Beam Systems, Nan Yao, Ed., *Cambridge University Press 2007, chapter 13, pp.337.*

70b-Nan Yao, “Introduction to the focused ion beam system” in Focused Ion Beam Systems, Nan Yao, Ed., *Cambridge University Press 2007, chapter 1, pp.1-29.*

70c- Hyoung Ho Kang, Clive Chandler, and Matthew Weschler, “ Gas assisted ion beam etching and deposition” in Focused Ion Beam Systems, Nan Yao, Ed., *Cambridge University Press 2007, chapter 3,pp.67-86.*

71- Graciela W. Padua, Qin Wang “Nanotechnology research methods for foods and bioproducts” *New York: John Wiley & Sons, Inc.2012, Chapter 11 by Yi Wang*

72- R. M. Langford, T.-X. Wang, D**.** Ozkaya, **“**Reducing the resistivity of electron and ion beam assisted deposited Pt” *Microelectronic Engineering, 84(5-8), pp. 784- 788, 2007.*

73- http://www.fei.com/products/dualbeams/quanta3d.aspx

74- J.E. Chandler, H.H. Messer and G. Ellender “Cytotoxicity of Gallium and Indium Ions Compared with Mercuric Ion” *Journal of Denalt Research 73(9), pp. 1554-1559, September, 1994.*

75- Sorab K.Ghandhi, “VLSI Fabrication Principles Silicon and Gallium Arsenide.” *New York: John Wiley & Sons, 1994, ch. 6, pp 368-383.*

76- http://www.gamry.com/products/potentiostats/reference-600/